Master Thesis

Engineering Myoglobin Towards Halogenase Activity

Written by

Marius Furter

under the supervision of

Matthias Tinzl

in the laboratory of

Prof. Donald Hilvert

Abstract:

Halogenated molecules serve as important synthetic intermediates and target compounds in medicine and agriculture [1]–[3]. Enzymatic catalysis could allow for stereo- and regioselective installation of halogen moieties from simple halides in aqueous media. However, few readily engineerable enzymes are available for this task. Based on its structural similarity to chloroperoxidase, we envisioned the heme-enzyme myoglobin as being capable of halogenations. To achieve initial activity, a series of variants based on myoglobin H64V V68A (Mb*) were generated by combinatorial means. First, an aspartate or glutamate was installed in either position 43, 64 or 68. Second, the proximal porphyrin-binding histidine (H93) was replaced by a cysteine. Third, the iron-protoporphyrin IX cofactor was replaced by a synthesized manganese-protoporphyrin IX. The produced variants were screened for chlorination activity by monochlorodimedone (MCD) assay. Mb*A68D showed the highest initial rate of up to 30 min^{-1}, matching that of the chloroperoxidase, albeit only for up to 12 turnovers per active site. Variants bearing a cysteine as proximal ligand, and those containing the manganese porphyrin showed lower activities than less modified variants. Because of mechanistic similarity of halogenation and peroxidase reactions, both proceeding though compound I, peroxidase activity was measured by guaiacol and vanillic acid assays and compared with halogenase activity. The strong linear correlation of initial rates during MCD and vanillic acid assays establishes a link between the two reactivities that can be exploited by discovering potent halogenases among known peroxidases.

Table of Contents

1. Introduction 3
1.1. Halogenation Reactions 3
1.2. Naturally Occurring Halogenases 4
1.3. Chloroperoxidase 6
1.4. Manganese Protoporphyrin IX Catalyzed Halogenations 8
1.5. Myoglobin 9
1.6. Project Aims 11
2. Results 12
2.1. Synthesis of Manganese Protoporphyrin IX 12
2.2. Molecular Cloning and Protein Production 12
2.3. Characterization of Variants 14
3. Discussion 22
3.1. Protein Expression and Porphyrin Loading 22
3.2. pH Stability of Mb* Variants 22
3.3. Rate of Compound I Formation 22
3.4. Bromination Activity 23
3.5. Halogenation Activity 23
3.6. Comparison of pH Optima for Halogenation Activity 24
3.7. Peroxidase Activity 24
4. Conclusion and Outlook 26
5. Materials and Methods 27
5.1. Molecular Biology 27
5.2. Protein Production 29
5.3. Activity Assays 30
5.4. Chemical Syntheses 31
6. Acknowledgements 32
7. References 33
8. Appendix 36
8.1. MS Data: Synthesized Protoporphyrin IX 36
8.2. MS Data: Synthesized Manganese$^{(III)}$-Protoporphyrin IX 37
8.3. Declaration of Independence 38

1. Introduction

1.1. Halogenation Reactions

Halogenated molecules are important as both synthetic precursors and target molecules [1]–[3]. In synthesis, they provide reactive handles for further functionalization through nucleophilic substitution or transition metal catalyzed cross-coupling reactions [1], [2]. In drugs, halogen content improves pharmacokinetics by increasing molecule lipophilicity while inhibiting oxidative metabolic degradation [3]. Furthermore, it also improves pharmacodynamics by mediating drug-receptor interactions by inductive effects and halogen bonding [4]. It is therefore unsurprising that a quarter of launched pharmaceuticals contain halogens, with over 16% bearing either iodine, bromine or chlorine [5] (*Figure 1-1*).

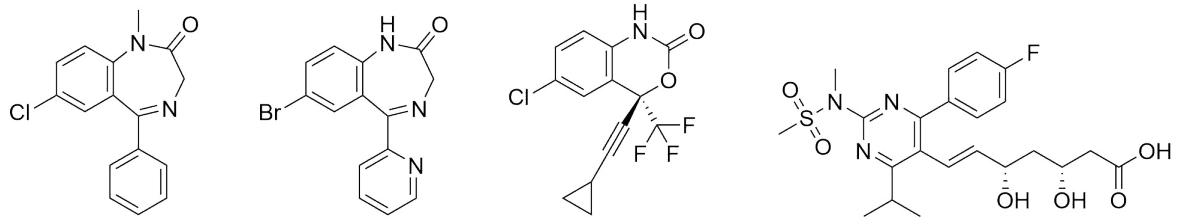

Diazepam Anxiety | **Bromazepam** Anxiety | **Efavirenz** Anti-retroviral | **Rosuvastatin** Statin

Figure 1-1 ***Examples of halogenated pharmaceuticals*** *including brominated, chlorinated and fluorinated compounds.*

For the applications described above, regioselective introduction of halogens is of the utmost importance. In synthesis, the position of the halogen will dictate where new bonds are formed, while in a drug candidate, the halogen must be located correctly to ensure the requisite supramolecular interactions. Thus, there is a need for robust, selective catalytic methods to achieve these ends.

Traditionally methods, such as the use of organo-halides together with Lewis acid catalysis, usually lack the desired degree of control. In general, halogenation is determined by the substrate and will occur at the most activated position. While it may be possible to overcome these difficulties by elegant synthetic planning, the lack of direct regiocontrol reduces synthetic utility.

Recently, progress in transition metal catalysis of halogenation reactions, as reviewed by Petrone *et al.* [6], has mitigated this issue. In addition to the electronic structure of the substrate, these catalysts use their numerous coordination sites to organize the geometry of both substrate and catalyst ligands. Spatial and electronic constraints then result in the regio- or stereoselective halogenation of the starting material, usually by an organohalide [6]. However, these reactions require the tedious preparation of both the catalyst and the organohalide reactants used. Furthermore, these methods rely on high catalyst loadings, often over 5 mol% [6]. Nonetheless, the extensive repertoire of available reactions remains impressive.

1.1.1 Enzyme Engineering Approaches

An alternative perspective on catalysis is provided by nature's enzymes. These protein catalysts selectively promote an incredibly diverse set of chemical transformations with high rates in aqueous media [7]. In cases where the 20 proteinogenic amino acids provide insufficient reactive possibilities, enzymes make use of cofactors. These include simple metal ions, metal porphyrins, PLP, thiamine, $FADH_2$ and NADH.

Biological chemists have long appreciated the unique advantages of enzymatic catalysis and have successfully tailored existing activities towards useful transformations by laboratory evolution [8], [9]. For example, an amine transaminase was engineered that can replace the transition-metal catalyst in the industrial-scale production of the diabetes drug sitagliptin [10]. Furthermore, protein engineers have been able to generate novel non-natural activities from extant enzymes by exploiting catalytic promiscuity [11]. Moreover, the

advent of computation assisted *de novo* design [12] is liberating protein engineers from the need to resort to structures evolved by nature. The range of interesting activities can be further increased by expanding the genetic code to non-natural amino acids [13] and by the use of novel cofactors [14]. Halogenations are among the many reactions that protein engineers are attempting to catalyze using enzymes [15]–[17]. When searching for specific activities, it is useful to survey what nature has achieved without human intervention.

1.2. Naturally Occurring Halogenases

The utility of halogenation has not gone unnoticed by nature. Nearly 5000 halogenated natural products have been identified to date [18]. The targets of these modifications range from simple alkanes through amino acids, terpenes and fatty acids, all the way to complex molecules like the bicyclic glycopeptide theopalauamide [19] (*Figure 1-2*). Both chlorinated and brominated natural products comprise over 1000 examples each. While chlorinated compounds dominate the terrestrial environment, brominated molecules are more abundant in marine organisms, presumably due to different halide availability. In contrast, less than 200 iodinated natural products [20] and only a dozen fluorinated compounds have been found [21].

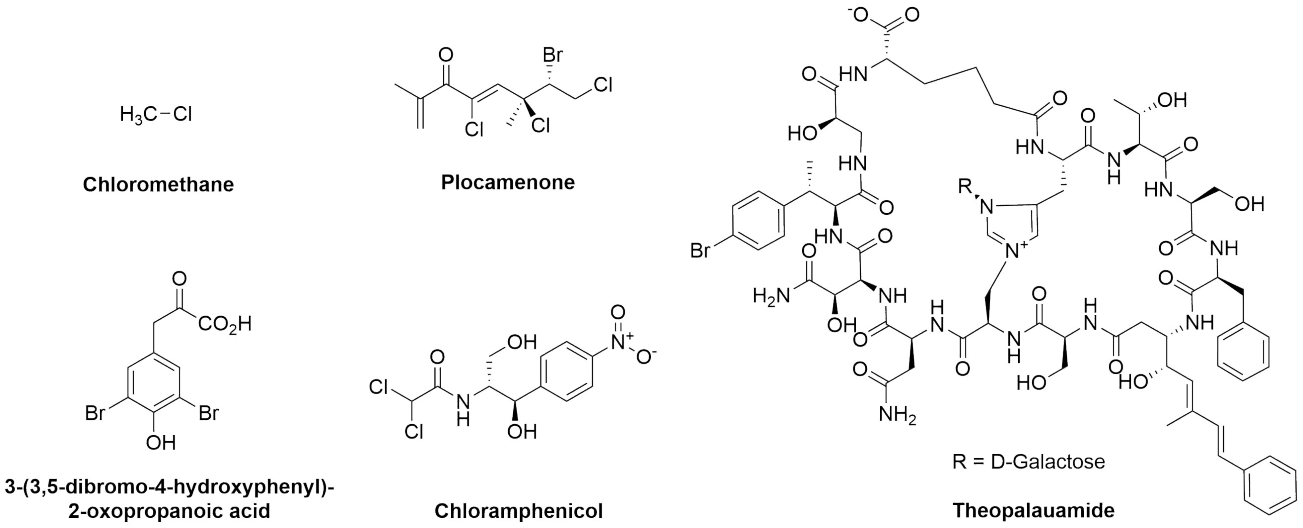

Figure 1-2 ***Examples of halogenated natural products*** *ranging from the simple to the complex.*

Nature must make do with the inert halide ions I^-, Br^-, Cl^- and F^- in the biosynthesis of halogenated molecules. The enzymes that achieve this feat can be divided into three mechanistic classes [22], [23] which will be referred to as class I,II and III in this work. Class I (heme-, vanadium- and flavin-dependent) enzymes catalyze the two-electron oxidation of halide (X^-) to a halonium (X^+) equivalent which takes the form of hypohalite (XO^-) in aqueous solution. The halonium equivalent can then take part in electrophilic substitution reactions, most frequently with aromatics. Class II (non-heme iron-dependent) enzymes facilitate the one-electron oxidation of halide to the $X^\bullet$ radical which can halogenate unactivated aliphatic carbon centers. Class III (nucleophilic) enzymes utilize halides as the nucleophile in an S_N2-type substitution reaction on electron-poor carbons. Only the class III enzymes are capable of fluorination, since their strategy avoids the need to overcome the high redox potential of fluorine. Nonetheless, the sizable enthalpic cost of fluorine desolvation must be paid [24].

Historically, the first halogenase to be identified was the *C. fumago* chloroperoxidase [25]. Following its discovery, a multitude of similar heme-dependent haloperoxidases were found. Haloperoxidases generate hypohalous acid as a halogenating agent for electron-rich substrates and thus belong to class I. The enzymes are grouped by the most electronegative halide they can activate, with variants capable of chlorination, bromination and iodination having been observed. Haloperoxidases can be divided into heme-iron-dependent and vanadium-dependent enzymes based on their respective cofactors.

Heme-iron-dependent haloperoxidases use hydrogen peroxide to form a heme-bound radical cation $Fe^{(IV)}$–oxo species known as compound I [23] (*Figure 1-3*). During this step an active site residue acts as a catalytic base. Compound I then oxidizes the halide to an enzyme bound heme-$Fe^{(III)}$-OX species, which can either react directly with the substrate or produce free hypohalous acid through protonation by the catalytic base. Due to the low selectivity of these enzymes it is likely that the hypohalous acid is freely diffusible, although the choice of mechanism may depend on substrate size and reaction conditions.

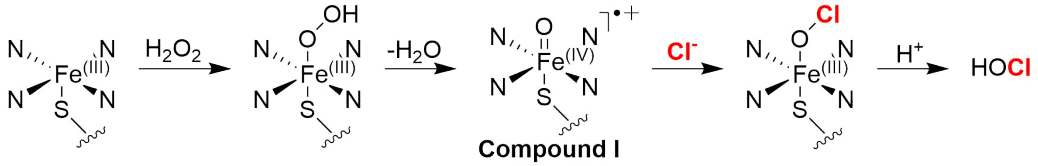

Figure 1-3 ***Mechanism of heme-iron-dependent peroxidases.*** *Adapted according to Latham 2018* [15].

In terms of engineering, the promiscuous activities that heme is capable of in these haloperoxidases are an attractive feature. Furthermore, the reactivity could be tuned by alteration of both the catalytic base and proximal ligand. The current lack of selectivity in many of these enzymes is a drawback. However, this may be overcome through the creation of dedicated substrate binding sites.

Vanadium-dependent haloperoxidases utilize a histidine-bound vanadate that is stabilized by three basic residues [15] (*Figure 1-4*). Hydrogen peroxide coordinates to the vanadium center by releasing water. This peroxo-vanadate is vulnerable to the attack of halide, forming an enzyme bound vanadium-OX species. It is surmised that these haloperoxidases also release free hypohalous acid in analogy with their heme-iron-dependent counterparts.

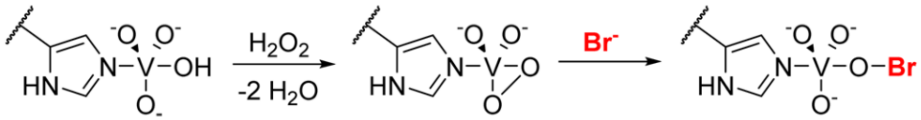

Figure 1-4 ***Mechanism of vanadium-dependent haloperoxidases****. Adapted from Latham 2018* [15].

α-Ketoglutarate (α-KG)-dependent halogenases are class II members. They use α-KG rather than heme to coordinate an iron that carries out the requisite redox chemistry. In contrast to haloperoxidases, they are capable of halogenating aliphatic carbons [15]. In the resting state, an $Fe^{(II)}$ is coordinated to the enzyme, α-KG and a halide (*Figure 1-5*, 1). Binding of molecular oxygen to the iron center leads to oxidative decarboxylation of α-KG. The resulting $Fe^{(IV)}$-oxo species (*Figure 1-5*, 2) then abstracts a hydrogen via a radical mechanism from the substrate, followed by recombination of the carbon-centered radical with the coordinated halogen [15] (*Figure 1-5*, 3). However, since most α-KG-dependent halogenases operate within the NRPS and PKS pathways, their substrates are generally tethered to acyl or peptidyl carrier proteins [15]. Furthermore, they need to be purified under inert conditions and perform fewer than 75 turnovers before oxidative inactivation [15]. Despite these difficulties, their radical mechanism remains attractive for synthetic applications.

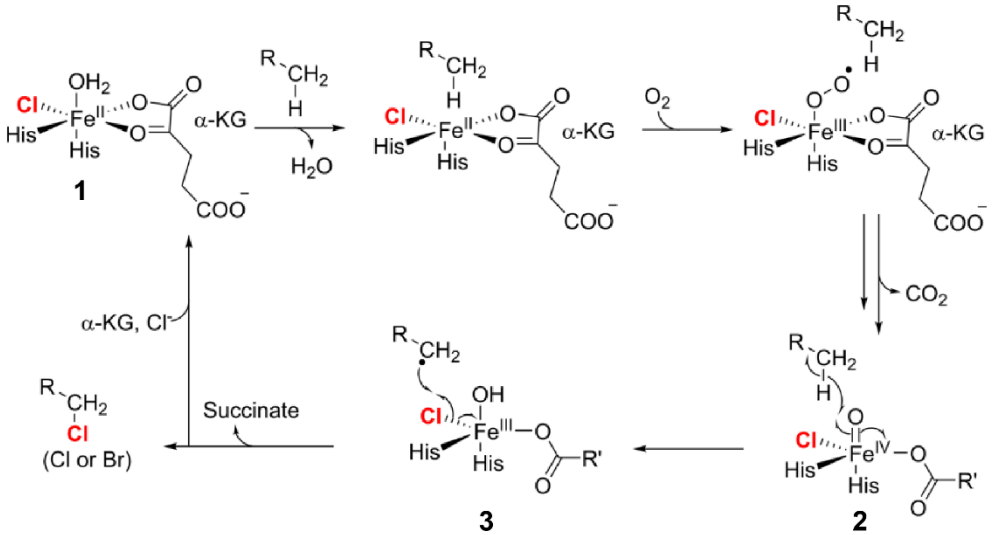

Figure 1-5 ***Mechanism of α-KG-dependent halogenases.*** *Adapted from Latham 2018* [15].

Flavin-dependent halogenases (Fl-Hals) are a sub-family of flavin dependent monoxygenases [17]. As such, they use reduced flavin ($FADH_2$) and molecular oxygen to produce C4a-hydroperoxyflavin (FAD-OOH) which is subsequently used to oxidize the halide (*Figure 1-6*). Their requirement for $FADH_2$ means they need to be coupled to a flavin reductase *in vivo* or have a continuous supply of the reduced cofactor *in vitro*. In the tryptophan halogenase PrnA, the substrate binding site is separated from the flavin binding site by a 10 Å tunnel, suggesting the need for diffusible hypochlorous acid. The sequestration of the substrate from the flavin cofactor seems essential for the enzyme to operate as a halogenase rather than a monooxygenase. Despite this constraint, Fl-Hals have been extensively investigated as biocatalysts for the regioselective halogenation of aromatic substrates [17]. Additionally, attempts have been made to change both substrate scope, regioselectivity, activity, and stability by rational and random mutagenesis approaches [17].

The first fluorinase to be structurally characterized, 5'-FDAS, stems from *Streptomyces cattelya* which secretes fluoroacetate and 4-fluorothreonin [24]. The enzyme was revealed to be able to catalyze fluorination of S-adenosyl methionine (SAM) to generate 5'-deoxy-5'-fluoroadenosine (FDA) through an S_N2-type mechanism (*Figure 1-7*). While this strategy overcomes the need to oxidize the highly electronegative fluorine, it still requires desolvation of fluoride for it to become a sufficient nucleophile. This is achieved by hydrogen bonding interactions with active site residues [24], [26]. Interestingly, several chlorinases have also been found that utilize a nucleophilic mechanism but are unable to catalyze reactions with fluoride [24]. The requirement for an excellent leaving group [24] in the substrate of these enzymes severely limits the possibility of engineering them for use in synthesis.

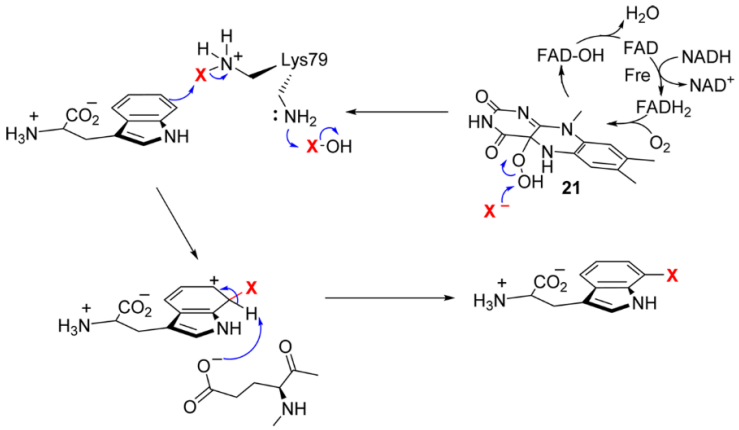

Figure 1-6 ***Mechanism of flavin-dependent halogenases.*** *Adapted from Latham 2018* [15].

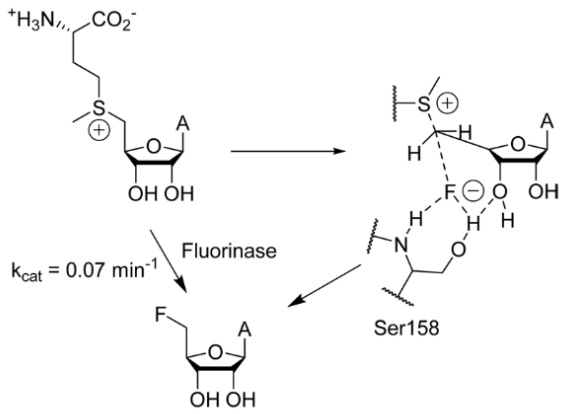

Figure 1-7 ***Mechanism of the* S. cattelya *fluorinase.*** *Adapted from Latham 2018* [15].

Based on this brief survey, heme- and flavin-dependent halogenases provide the most attractive targets for engineering attempts. While Fl-Hals have received much attention in recent years [17], heme-dependent haloperoxidases remain the most thoroughly investigated class for historical reasons.

1.3. Chloroperoxidase

Chloroperoxidase (CPO) is a 42 kDa heme-iron-dependent haloperoxidase found in the marine fungus *Caldariomyces fumago* where it is responsible for the dichlorination of 1,3-cyclopentanedione in the biosynthesis of caldariomycin [27] (*Figure 1-8*). CPO is heavily glycosylated with the major isozyme containing three N-glycosylation and several O-glycosylation sites making up 18% of its molecular weight [28]. Chloroperoxidase has been transformed into *E. coli*. However, periplasmic expression yielded apo-enzyme, which could only be reconstituted to the holo-form in 5% yield [29]. Though it seems that glycosylation is not strictly necessary for refolding. The low efficiency of the process combined with its laboriousness excludes this method from use in enzyme engineering. More recently, fully active recombinant chloroperoxidase has been efficiently expressed in the filamentous fungi *Aspergillus niger*, opening the door for mutagenesis studies [30].

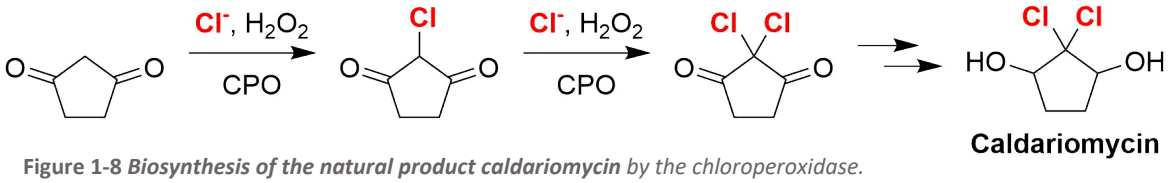

Figure 1-8 ***Biosynthesis of the natural product caldariomycin*** *by the chloroperoxidase.*

The crystal structure of CPO has been determined by X-ray spectroscopy [31] (*Figure 1-9*). The chloroperoxidase relies on an iron protoporphyrin IX cofactor for its function. The heme is sandwiched between N- and C-terminal domains which consist mostly of α-helices. Cysteine 29 acts as proximal ligand, while the two remaining cysteines form a disulfide bond. Like CPO, cytochrome P450 also uses cysteine as proximal ligand, giving rise to UV/VIS spectroscopic resemblance [32]. The active site of CPO (*Figure 1-16*) is located deep within the enzyme and can only be accessed through a hydrophobic channel. It is fairly polar, with glutamate 183 playing the role of the acid-base catalyst in deprotonating H_2O_2. Histidine 105 probably serves to orient glutamate 183 and modify its pKa. In free solution the side chain of glutamate has a pKa of 4.2, but the low pH optimum of the chloroperoxidase (below 4) suggests that this value is perturbed downward in the enzyme.

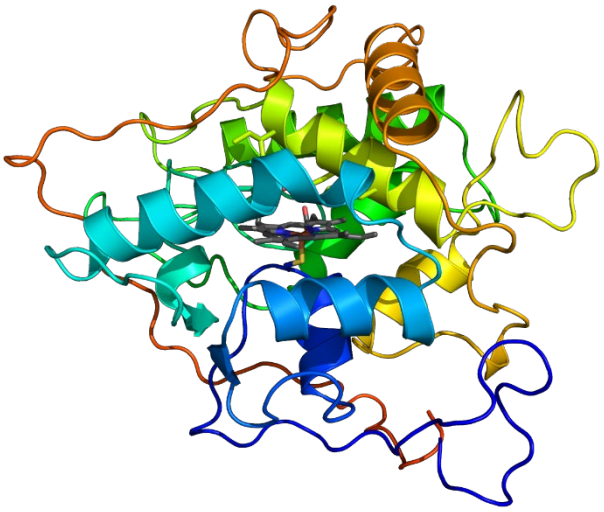

Figure 1-9 ***Crystal structure of the C. fumago chloroperoxidase*** **(PDB** 1CPO) *with its porphyrin cofactor* ***(grey)****.*

Chloroperoxidase catalyzes the hydrogen peroxide dependent oxidation of I^-, Br^- and Cl^-. This is achieved via the formation of the $Fe^{(IV)}=O^{+\bullet}$ species called compound I. The radical cation is two oxidation equivalents above the resting state. It can either be reduced in a two-electron process in halogenation (halide) and catalase (H_2O_2) reactions or can be reduced in two separate one-electron transfers from peroxidase substrates, via compound II ($Fe^{(IV)}=O$). A corresponding catalytic cycle has been proposed [33] (*Figure 1-12*).

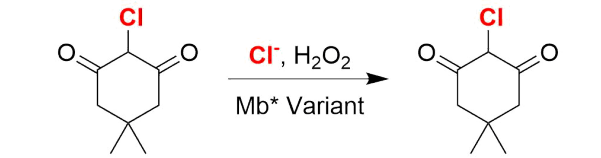

Figure 1-10 ***Monochlorodimedone assay reaction.***

The activity of CPO is benchmarked by the monochlorodimedone (MCD) assay [34] (*Figure 1-10*) in which the decrease of substrate absorbance is monitored spectroscopically. MCD, which resembles the enzyme's natural substrate, is chlorinated to yield dichlorodimedone, which absorbs at a different wavelength. Aside from MCD, CPO is capable of dihalogenating alkenes and alkynes as well as generating α,β-halohydrins [35]. Furthermore, it can generate α-halogenated ketones from alkynes [36]. Finally, it is capable of halogenating anilines [37], substituted phenols and β-keto acids among others [38] (*Figure 1-11*).

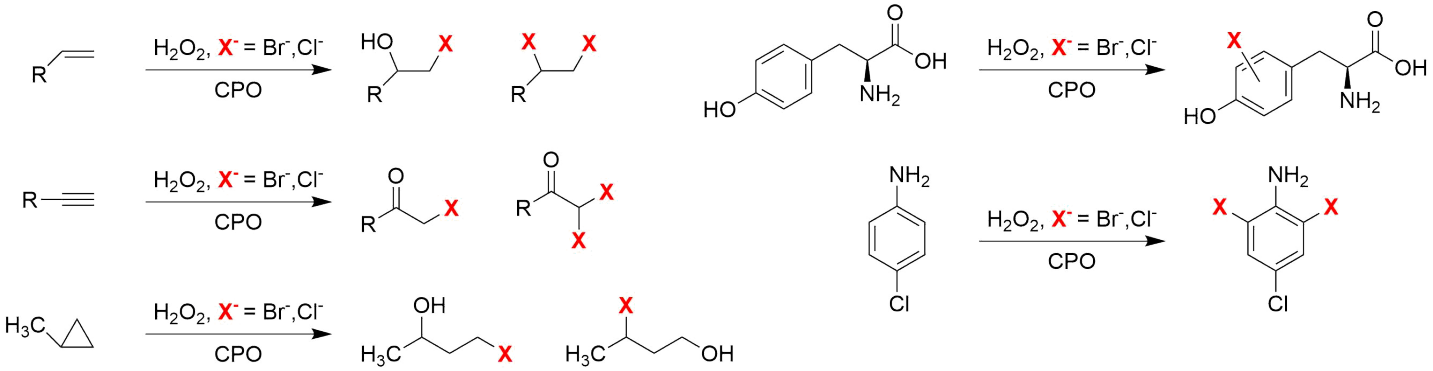

Figure 1-11 ***Examples of halogenation reactions catalyzed by the chloroperoxidase****.*

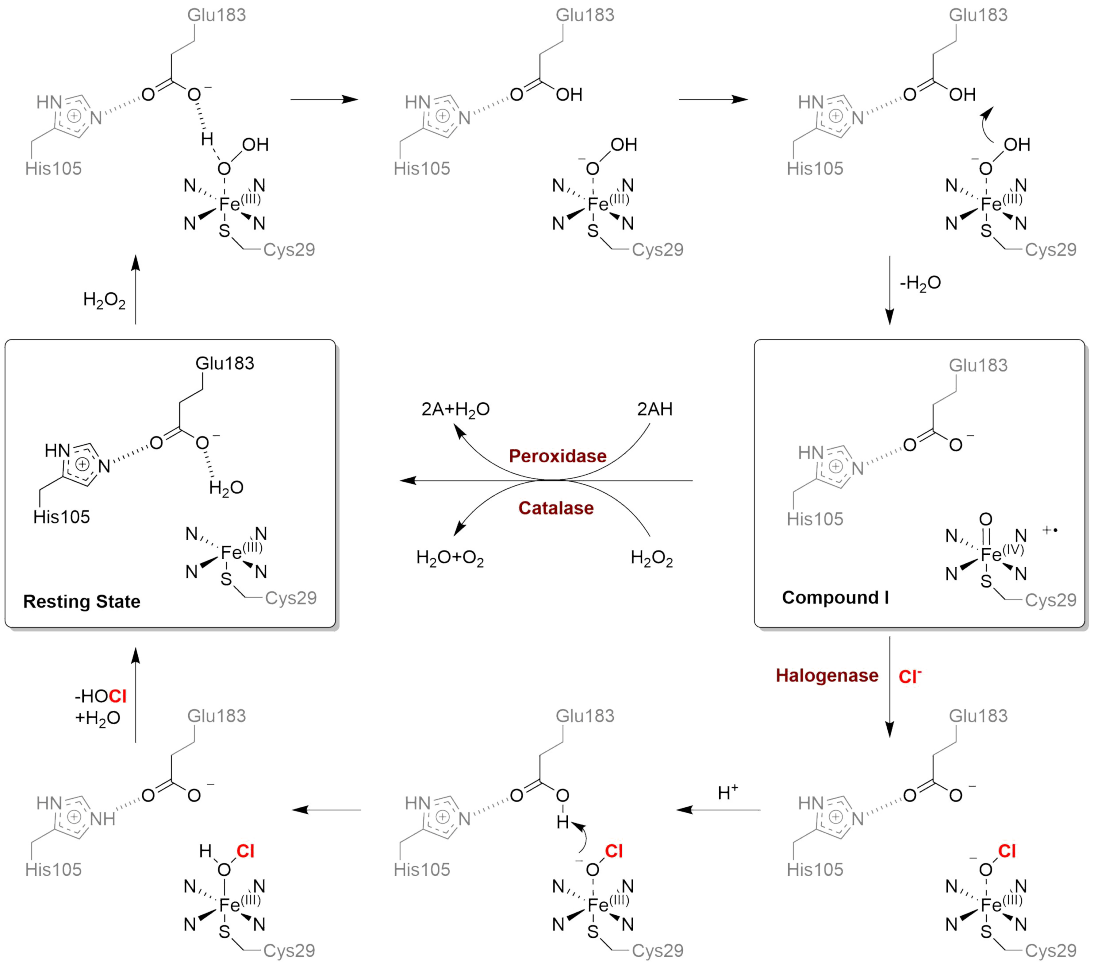

Figure 1-12 ***Catalytic cycle of the chloroperoxidase*** *during halogenase, peroxidase and catalase reactions. Adapted according to* [33].

In addition to its halogenase activity, CPO can oxidize typical peroxidase substrates such as guaiacol [39]. Furthermore, it is capable of H_2O_2 dismutation [39]. CPO also catalyzes many P450 reactions, notably hydroxylation, oxygen transfers to several acceptors, and stereoselective epoxidation. The pH optimum for reactions using halide is below 4, while it ranges from 4-7 in peroxidase reactions [39].

1.4. Manganese Protoporphyrin IX Catalyzed Halogenations

Inspired by the reactivity of heme enzymes, Liu *et al.* reported the regioselective chlorination of aliphatic substrates using the bulky Mn(TPP)Cl porphyrin in catalytic quantities together with aqueous hypochlorite in a biphasic system [40]. Previous work with the catalyst had demonstrated its ability to oxygenate aliphatic substrates under similar conditions [41], presumably through a cytochrome P450-like radical oxygen rebound mechanism [42]. The manganese porphyrin catalyst would have to proceed through a similar L-$Mn^{(IV)}$-OH intermediate to perform the chlorination reaction (*Figure 1-13*). The switch in solvent system, however, seemed to bias the reaction away from the more rapid oxygenation and towards halogenations. Further investigation revealed that the addition of ligands such as imidazole or pyridine significantly decreased the proportion of chlorinated products. This underscores the importance of the coordinated ligand for determining the reaction trajectory, with electron-rich ligands such as hydroxide and fluoride slowing down the oxygen rebound mechanism and therefore promoting halogenations.

Based on these findings, *Liu et al.* successfully expanded this reactivity to fluorination reactions using the same Mn(TPP)Cl catalyst [43]. In this work, silver fluoride was used together with iodosylbenzene as the oxidant in

a homogenous solvent system. These conditions were able to regioselectively fluorinate a diverse set of aliphatic substrates in yields above 50%. Based on mechanistic studies and DFT calculations, a *trans*-difluoro species $Mn^{(IV)}(TMP)F_2$ was postulated as the key intermediate in the proposed catalytic cycle (*Figure 1-14*). The presence of the fluorine ligand was again hypothesized to be essential for steering the reactivity away from oxygenation and towards halogenation. Similar manganese porphyrins have also been incorporated in enzymes. In particular, they are capable of altering the promiscuous activities of myoglobin [44]–[46].

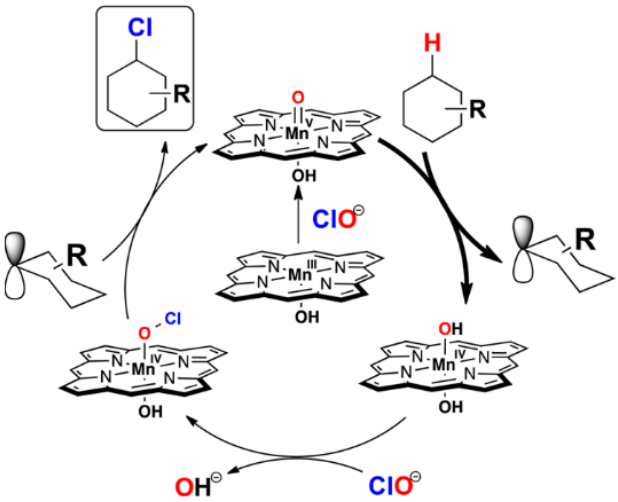

Figure 1-13 ***Proposed catalytic cycle for manganese porphyrin catalyzed chlorinations.*** *Adapted from Liu 2015* [64]

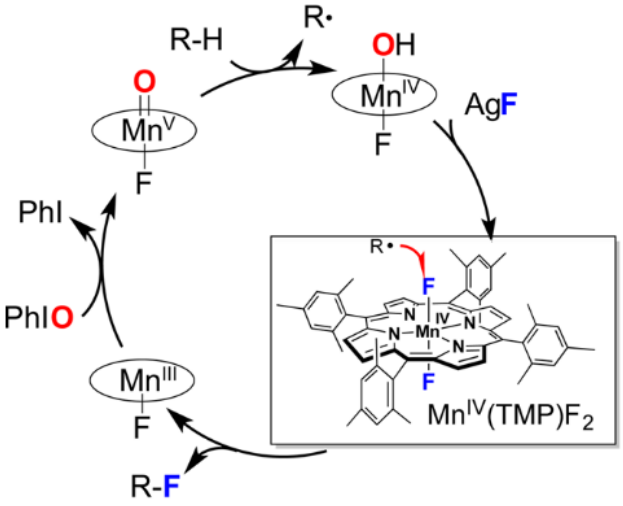

Figure 1-14 ***Proposed catalytic cycle for manganese porphyrin catalyzed fluorinations*** *including the postulated* trans*-difluoro intermediate* ***($Mn^{IV}(TMP)F_2$).*** *Adapted from Liu 2015* [64]

1.5. Myoglobin

Myoglobin is a heme-protein responsible for buffering the oxygen concentration in respiring tissues [47]. Its affinity for oxygen therefore lies between that of bloodborne hemoglobin and the cytochromes of the respiratory chain. Myoglobin homologues have been found in all three kingdoms that bind heme in a similar manner but possess different biological functions. The 17 kDa sperm whale myoglobin was the first to be recombinantly expressed in *E. coli* [48] with 10% of the total soluble protein being holo-myoglobin. The protein absorbs strongly in the blue region with a Soret band between 400-410 nm. Its oxidation state can be discerned by eye, with freshly purified protein being blood red ($Fe^{(II)}$) and slowly turning brown as it oxidizes ($Fe^{(III)}$) over the course of days. The heme-iron can be reduced by using dithionite [47].

The x-ray structure of myoglobin was first solved in 1960 [49] being the first protein structure to be resolved at the atomic level (*Figure 1-15*). It is composed of 8 α-helices arranged in what has come to be known as the globin fold. The myoglobin heme group is wedged into a central hydrophobic pocket where it is coordinated by the Nε of the proximal histidine (H93). Its active site (*Figure 1-16*) also contains a second distal histidine (H64) which aids oxygen binding.

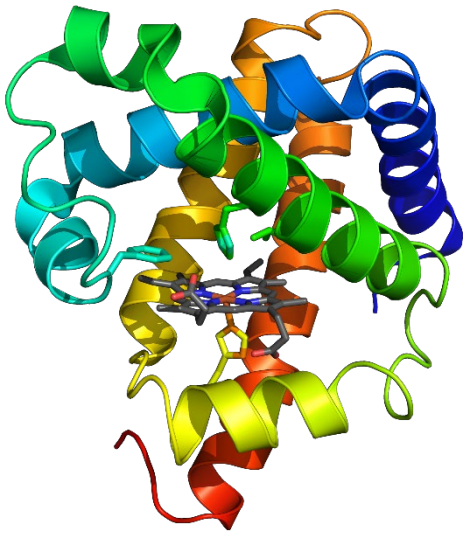

Figure 1-15 ***Crystal structure of sperm whale myoglobin*** **(PDB** 1VXA) *with its porphyrin cofactor* ***(grey)***.

A comprehensive mutagenesis study describing which residues are required for heme binding has been conducted [50]. Unsurprisingly, H93 mutation leads to the largest increase in dissociation of the cofactor. Furthermore, L89 also causes over 100-fold increased rate of hemin loss. Notably for the following work, perturbation of F43, even by apolar residues leads to increases in dissociation of over 10-fold. Position V68 seems to be able to accept all substitutions well, with little difference being observed between V68L and V68W. Mutating H93G leads to a cavity mutant where exogenous proximal ligands of choice can be investigated [51]. Adding imidazole mimics the wild-type enzyme.

Myoglobin shows considerable structural similarity to the chloroperoxidase (*Figure 1-16*). Their active sites both contain a porphyrin cofactor but differ in terms of proximal ligand and active site base. While myoglobin uses a histidine (H93) to coordinate its heme cofactor, the chloroperoxidase uses a cysteine instead. Furthermore, myoglobin additionally possesses an active site distal histidine (H64) while the chloroperoxidase bears an active site glutamate that acts as a catalytic base during halogenation reactions.

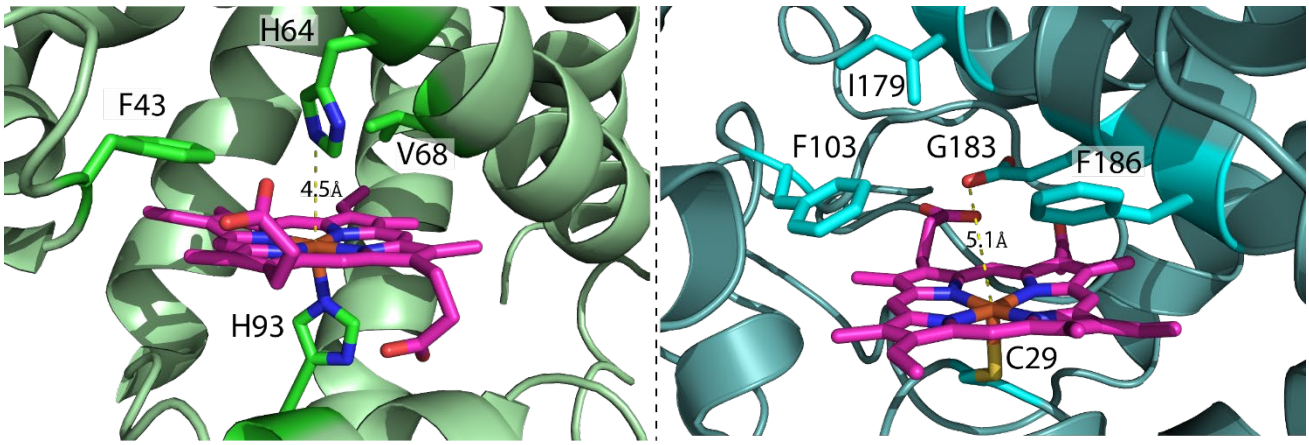

Figure 1-16 ***Comparison of myoglobin (left,*** **PDB** 1VXA***) and chlorperoxidase (right,*** **PDB** 1CPO***) active sites*** *highlighting key residues.*

Since the iron porphyrin readily binds many ligands including dioxygen, CO, NO, F^-, Cl^-, CN^-, N_3^- and OH^- [47], myoglobin has proven to be able to catalyze a diverse set of chemistries. Notably, myoglobin variants, along with other heme proteins, react with diazo esters to yield an iron carbenoid intermediate which has been characterized by X-ray crystallography [52], [53]. This activity allows myoglobin to perform carbene chemistry including cyclopropanations, N-H insertions, S-H insertions, aldehyde olefinations and (with a manganese or iridium substituted cofactor) C-H insertions (reviewed in [54], [55]) (*Figure 1-17*). Additionally, myoglobin variants are also capable of catalyzing some nitrene insertion reactions (*Figure 1-17*). Myoglobin also possesses low levels of promiscuous peroxidase activity which has been exploited to generate an evolved variant capable of natural peroxidase-like rates and total turnover numbers [56].

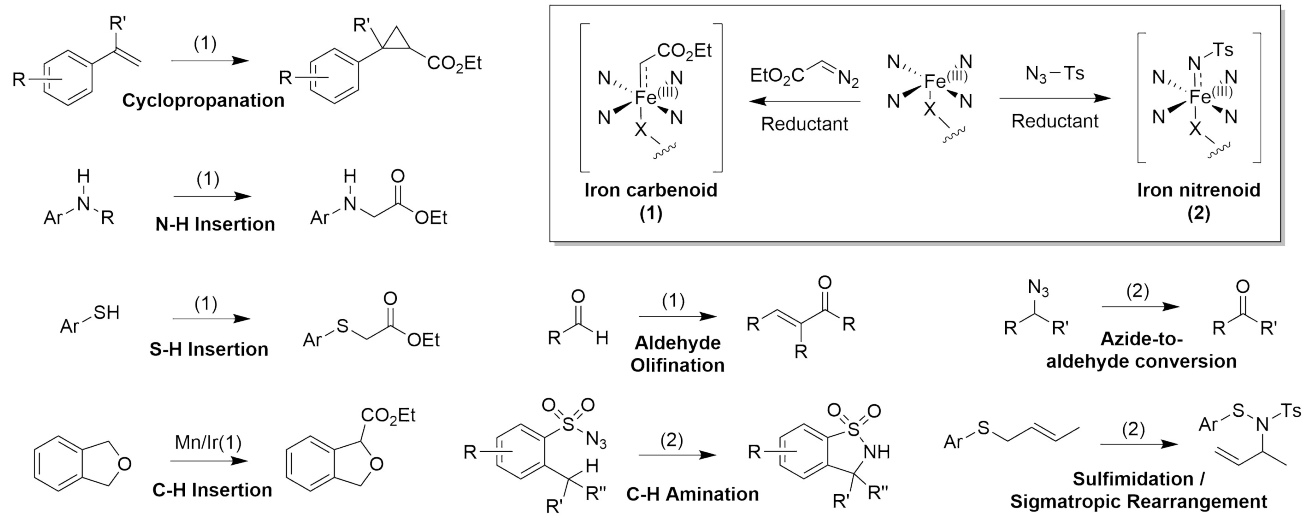

Figure 1-17 ***Examples of reactions catalyzed by myoglobin variants*** *via iron carbenoid* ***(1)*** *or iron nitrenoid* ***(2)*** *intermediates.*

Heme-proteins offer the advantage of allowing engineering by both genetic and synthetic mechanisms. In addition to mutating the protein, alternative non-natural cofactors may be installed. For example, manganese protoporphyrin IX reconstituted myoglobin variants display altered reactivity in both carbene insertion [44] and alkene epoxidation reactions [45]. In these systems, active site residues can aid and perturb the cofactor's reactivity. Enzymatic activity can be subsequently fine-tuned by laboratory evolution.

1.6. Project Aims

The aim of this project is to create a halogenase based on myoglobin. Such an enzyme would be more amenable to engineering and mechanistic investigation than naturally occurring enzymes such as the chloroperoxidase. This goal seems feasible due to the broad range of activities in heme-proteins including halogenation, as well as the structural similarities between myoglobin and the chloroperoxidase. To further increase this structural resemblance, myoglobin variants that contain aspartate or glutamate in either position 43, 64 or 68 were to be generated. Furthermore, for each of these variants, a mutant was to be made containing a cysteine as proximal ligand in position 93 instead of the natural histidine ligand. Additionally, the potential benefits of incorporating a manganese porphyrin IX suggested by the reports of Liu *et al.* [40], [43] were to be investigated.

Like the chloroperoxidase, a myoglobin derived halogenase would presumably operate via compound I. The generated variants could thus be used to link halogenase activity to other activities requiring this key intermediate. Specifically, peroxidase activity was to be examined. If a link between halogenase and peroxidase activity could be established, it would transform the extensive literature on peroxidases into a source for discovering novel halogenases.

2. Results

2.1. Synthesis of Manganese Protoporphyrin IX

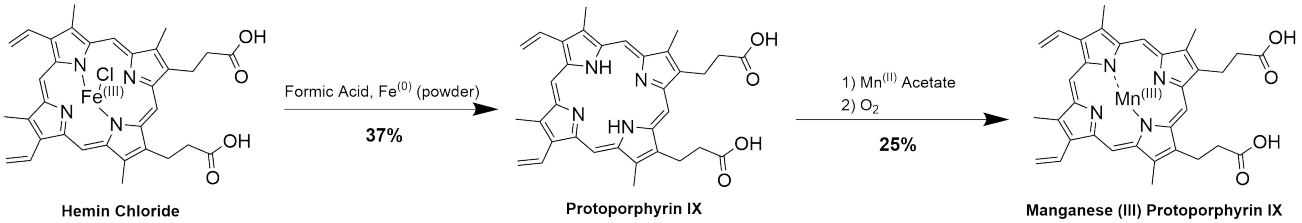

Scheme 2-1 ***Synthesis of manganese protoporphyrin IX from hemin chloride.***

Manganese protoporphyrin IX was synthesized from hemin chloride in two steps. First, hemin chloride was converted to protoporphyrin IX (*Scheme 2-1*) in 37 % yield. The product was characterized by UV/VIS spectroscopy (*Figure 2-1*, middle) and mass spectroscopy (Appendix 8.1). The spectrum of the synthesized product shows the same peaks as commercial protoporphyrin IX (*Figure 2-1*, middle). The absorbance peak at 250 nm stems from residual pyridine. Based on comparison of the UV/VIS spectra of commercial product with the synthesized product, the purity was estimated to be 80 %.

In the second step, protoporphyrin IX was converted to manganese protoporphyrin IX (*Scheme 2-1*) in 25 % yield at 60 % conversion. The product was characterized by UV/VIS spectroscopy (*Figure 2-1*) and mass spectrometry (Appendix 8.2). The purity of the product was estimated to be 60 % based on the UV/VIS spectra. No further attempts were made at purifying the product, since it was assumed to be unlikely that protoporphyrin IX would be incorporated into the enzyme.

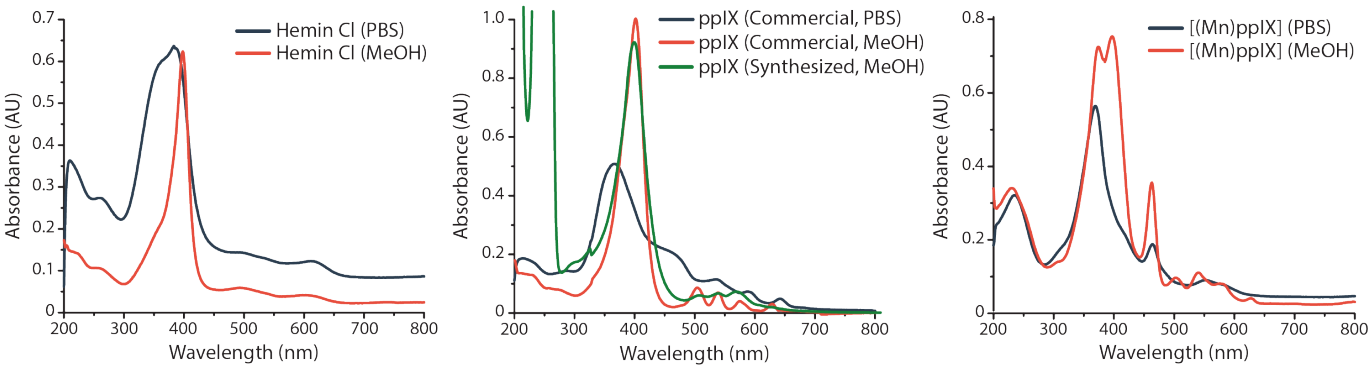

Figure 2-1 ***UV/VIS spectra*** *of hemin chloride in PBS* ***(left, blue)*** *and methanol* ***(left, red)****, synthesized protoporphyrin IX in methanol* ***(middle, green)****, commercial protoporphyrin IX in PBS* ***(middle, blue)*** *and methanol* ***(middle, red)****, and synthesized manganese protoporphyrin IX in PBS* ***(right, blue)*** *and methanol* ***(right, red)****.*

2.2. Molecular Cloning and Protein Production

2.2.1 Generation of Mb* Variants

A series of enzymes based on sperm whale myoglobin were generated. A previously investigated variant, Mb* (PDB: 6G5T, see Materials and Methods for sequence), containing two mutations H64V and V68A along with a His-tag was used as a starting point for further diversification. This starting scaffold, which lacks a potential catalytic base for haloperoxidase-like activity, was modified in accordance with the project aims (Section 1.6) through iterated quickchange PCR (*Table 5-1)*. First, a new potential catalytic base (aspartate or glutamate) was installed in either position 43, 64 or 68. Second, the proximal heme-binding ligand (H93) was exchanged for a cysteine. Combination of these two strategies yielded 14 Mb* variants (*Table 2-1*).

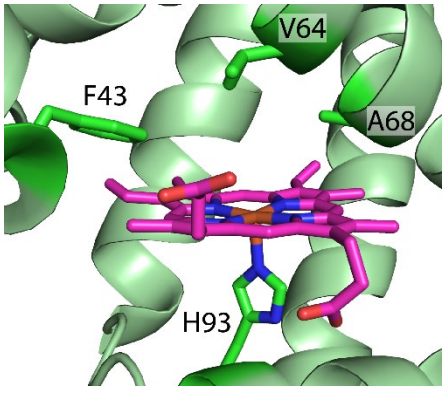

Figure 2-2 ***Mb**** **(PDB** 6G5T**)** ***active site*** *indicating the residues mutated to obtain the investigated variants.*

Additionally, the cavity mutant Mb*H93G, which lacks a proximal ligand altogether, was generated. Each sequence was successfully verified prior to transformation into the expression strain.

2.2.2 Protein Expression

The Mb* variants were expressed in BL21 *E. coli.* Following sonication, the lysate was supplemented with hemin chloride to ensure maximal porphyrin loading. The proteins were purified by Nickel-NTA, dialyzed against PBS, and further purified by size exclusion chromatography.

All of the expressed variants showed the expected mass on SDS, with faint dimer bands being visible in some cases (*Figure 2-3*). Protein yields (*Table 2-1*) were acceptable, except for F43D/E which expressed poorly. Variants bearing cysteine as the proximal ligand (H93C) showed low porphyrin loading between 2% and 4%. Consequently, their yields based on porphyrin absorbance were also lower. Nonetheless, it was possible to produce enough protein to conduct the necessary experiments. The cavity mutant, Mb*H93G, incorporated less than 1% of porphyrin and was excluded from further investigation.

A surprising amount of protein was lost during the size exclusion chromatography step. In most cases only around 60% of protein could be recovered. Presumably, a significant fraction of the protein aggregated during the spin filtration prior to injection. Size exclusion purification only led to an increase in porphyrin loading of a few percent.

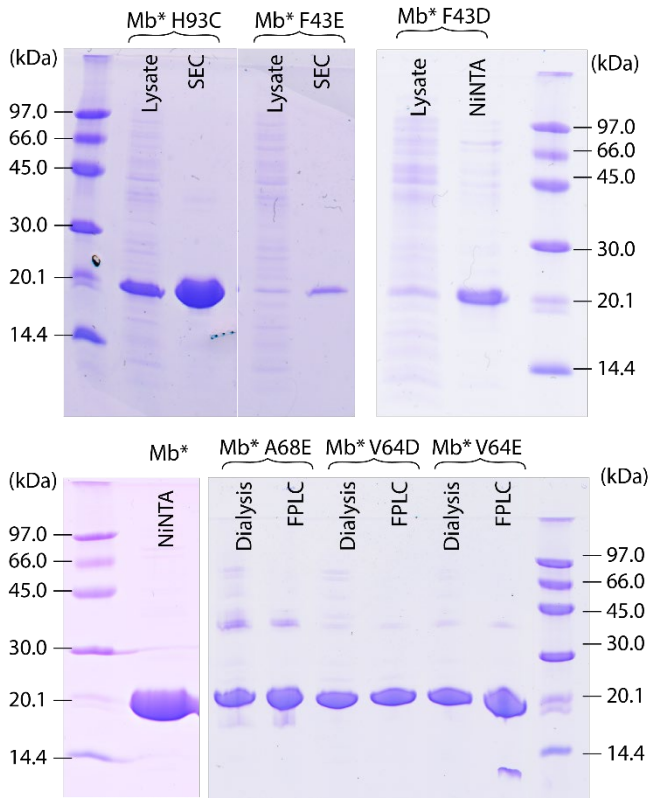

Figure 2-3 ***Representative SDS-PAGE*** *gels of the expressed Mb* variants.*

Variant	Yield (mg/L)	Loading
Mb*	19.3 [a]	17%
Mb* H93C	1.6[a]	2%
Mb* V64Da	20.1[a]	25%
Mb* H93C V64D	4.2[a]	4%
Mb* V64E	14.7[a]	14%
Mb* H93C V64E	2.8[a]	4%
Mb* F43D	n.d	n.d
Mb* H93C F43D	n.e.	n.e.
Mb* F43E	0.3[b]	18%
Mb* H93C F43E	n.e.	n.e.
Mb* A68D	4.8[b]	47%
Mb* H93C A68D	n.e.	n.e.
Mb* A68E	20.2[a]	26%
Mb* H93C A68E	n.e.	n.e.
Mb* H93G	0.3[b]	<1%

Table 2-1 ***Cloned Mb* variants*** *with expression yield after dialysis* ***(a)*** *or SEC* ***(b)*** *based on porphyrin absorbance along with corresponding porphyrin loading percentages. Several variants were never expressed* ***(n.e.)****. Mb*F43D was expressed, but no yield was determined* ***(n.d.)****.*

2.2.3 Incorporation of Manganese Porphyrin

The synthesized manganese protoporphyrin IX (Section 2) was incorporated into representative Mb* variants (*Table 2-2*) in two steps. First, the existing iron porphyrin was extracted using organic solvent under reduced pH, followed by size exclusion chromatography. Second, the resulting apo-protein was reconstituted by incubation with an excess of the manganese porphyrin, followed again by size exclusion chromatography. The process was validated by comparison of the UV/VIS spectrum of Mb*[(Mn)ppIX] to a literature spectrum (*Figure 2-4*).

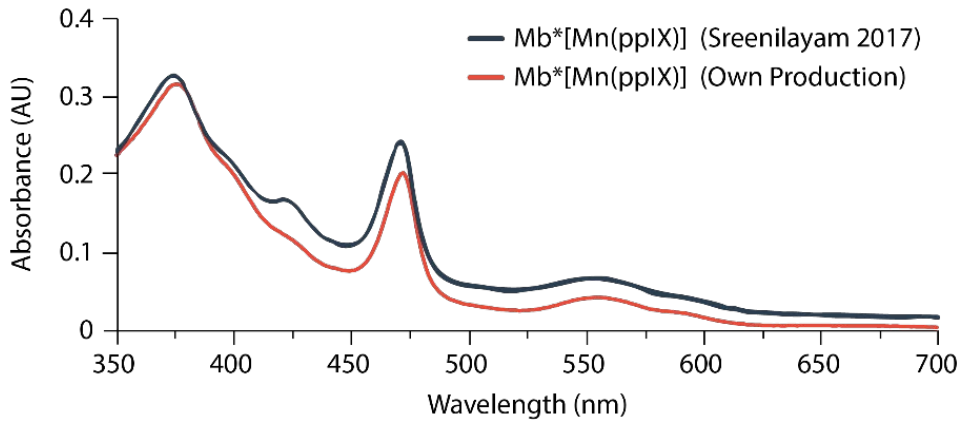

Figure 2-4 *Comparison of literature manganese porphyrin Mb* UV/VIS spectrum* ***(black,*** [44]***)*** *with corresponding enzyme from own production* ***(red)****.*

The efficiency of both apo-protein production and porphyrin incorporation steps are listed in Table 2-2. Apo-protein was produced with a large variation in efficiency between 7% and 50% while incorporation proceeded at an acceptable yield of 33-63%. The manganese porphyrin loading proved to be comparable to the loading of iron porphyrin in most cases. Remarkably, in the case of Mb*[(Mn)ppIX] the loading increased dramatically from 2% to 16%.

Variant	Apo Efficiency	Incorporation Efficiency	Initial Loading	Final Loading
Mb* [(Mn)ppIX]	31%	42%	25%	11%
Mb* H93C [(Mn)ppIX]	50%	33%	2%	16%
Mb* V64D [(Mn)ppIX]	15%	63%	28%	23%
Mb* H93C V64D [(Mn)ppIX]	7%	54%	4%	2%
Mb* V64E [(Mn)ppIX]	28%	50%	23%	26%

Table 2-2 ***Porphyrin extraction and incorporation efficiencies*** *in the production of manganese porphyrin Mb* variants including initial and final loading percentages.*

2.3. Characterization of Variants

2.3.1 UV/VIS Characterization

All expressed Mb* variants were characterized by UV/VIS spectroscopy (*Figure 2-5*). Variants containing histidine as the proximal ligand showed a Soret band between 408 and 410 nm while those containing a cysteine had a blue-shifted Soret band between 380 and 400 nm. In all cases, the presence and position of the catalytic base had little influence on the spectra. However, the position of the Soret band in the cysteine variants seemed to vary with protein age. This was presumably due a progressive change in the oxidation state of the iron porphyrin [57]. All manganese porphyrin variant spectra were indistinguishable, regardless of proximal ligand.

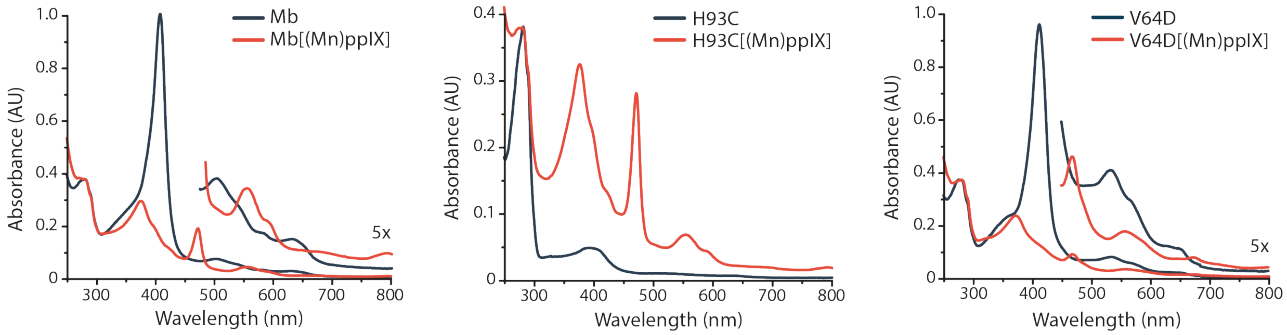

Figure 2-5 ***UV/VIS spectra of Mb* variants*** *showing comparisons between Mb* and Mb*[(Mn)ppIX]* ***(left)****, Mb*H93C and Mb*H93C[(Mn)ppIX]* ***(middle)*** *as well as Mb*V64D and Mb*V64D[(Mn)ppIX]* ***(right)****.*

2.3.2 Temporal Stability

While performing experiments, a noticeable loss of initial rate (up to 60%) in the MCD assay (Section 2.3.6) of Mb*V64D was observed over the course of several weeks. This effect had not been observed during previous work with myoglobin variants (Matthias Tinzl). Consequently, many of the experiments were repeated with a fresh batch of enzyme that was immediately flash frozen and stored at -80°C for future use. To investigate the decline in rate over time, the rates of freshly thawed Mb*V64D and Mb*A68D were compared to rates obtained after storing the same enzymes for two weeks at 4°C (*Figure 2-6*). However, in this systematic experiment, no significant loss in rate or total turnover number was observed over time.

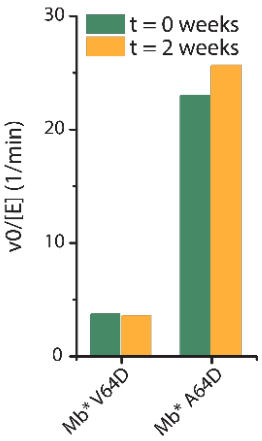

Figure 2-6 ***Temporal stability of initial rate of Mb*V64D and Mb*A68D in the MCD assay*** *using 20 µM MCD, 20 mM KCl, 0.5 mM H_2O_2 and 0.5 µM enzyme at pH 5.5 directly after thawing* ***(green)*** *and after 2 weeks at 4°C* ***(orange)****.*

2.3.3 pH Stability

The pH stability of four Mb* variants was assessed by measuring UV/VIS spectra in buffers of varying pH (*Figure 2-7, Figure 2-8*). The resulting spectra shifted from the native spectrum to a spectrum that resembles hemin chloride in aqueous solution (*Figure 2-7*, left) at a critical pH value. This was interpreted as the porphyrin no longer being bound in the enzyme active site past this threshold. In the case of Mb*, this shift takes place below pH 4.5, for Mb*V64D, it takes place below pH 4 and with Mb*H93C V64D, it takes place below pH 3. The pH stability of Mb*V64D [(Mn)ppIX] could not be determined by this method, since the protein spectrum is similar to the spectrum of the manganese porphyrin in aqueous solution.

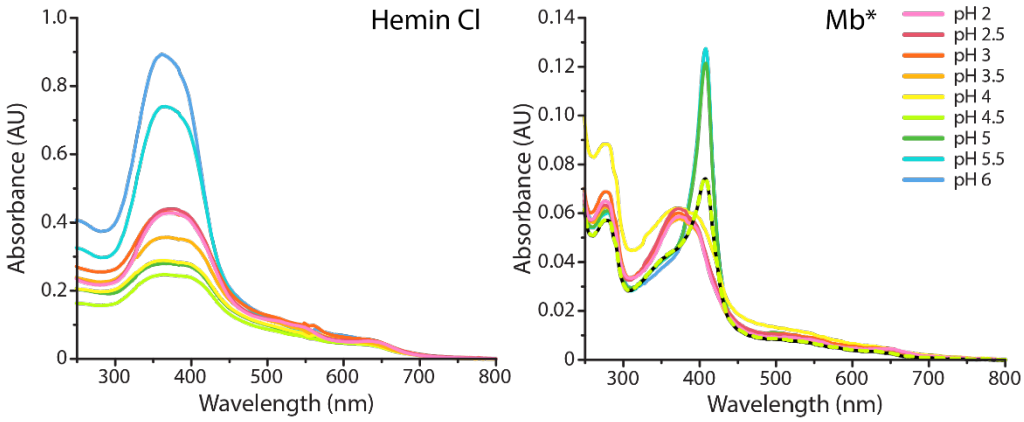

Figure 2-7 ***pH dependence of UV/VIS spectra*** *of hemin chloride* ***(left)*** *and Mb* **(right)**. The threshold pH values are indicated by dashed lines where applicable.*

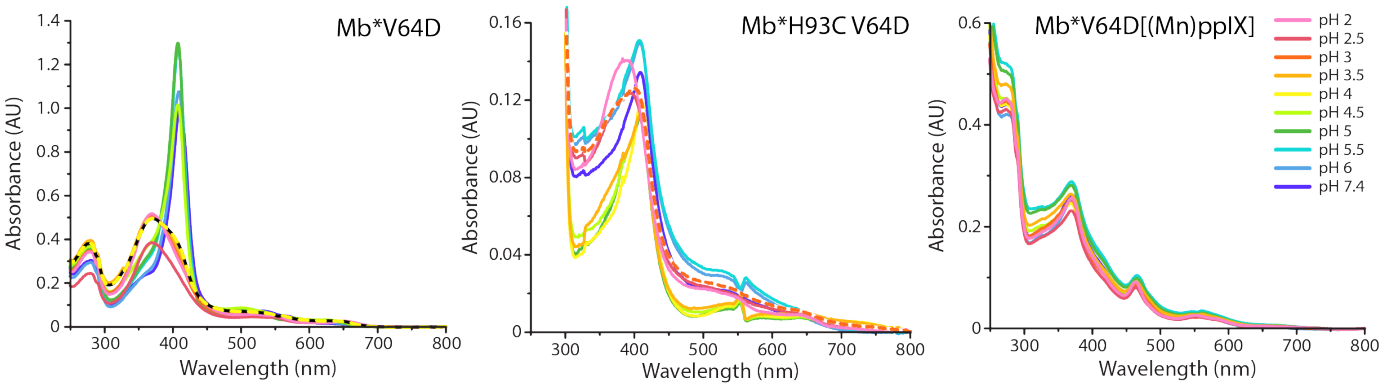

Figure 2-8 ***pH dependence of the UV/VIS spectra*** *of Mb*V64D* ***(left)****, Mb*H93C V64D* ***(middle)*** *and Mb*V64D[(Mn)ppIX]* ***(right)****. The threshold pH values are indicated by dashed lines where applicable.*

2.3.4 Compound I Formation

The UV/VIS spectra of four variants were monitored upon addition of either mCPBA or hydrogen peroxide. In the case of all iron porphyrin variants, a decrease in the Soret band was observed over several minutes upon addition of either oxidant. Additionally, there was a 2-4 nm red-shift of the peak. The decrease was more rapid in variants containing a catalytic base (*Figure 2-9*, middle, left) than in those without (*Figure 2-9*, left), even when only 140 µM hydrogen peroxide was used for the former, instead of 3.5 mM. Furthermore, the rate of decrease of the Soret band was proportional to the observed halogenation activity in the MCD assay (Section 2.3.6). It is difficult to tell definitively whether compound I was indeed formed as its absorbance maximum (421 nm [58]) is very close to that of the Soret band. Furthermore, it is also possible that compound II is directly formed, as it also possesses a similar absorbance maximum (422 nm [59]). The obtained spectra did not resolve the Q-bands well enough to enable any distinction based on them.

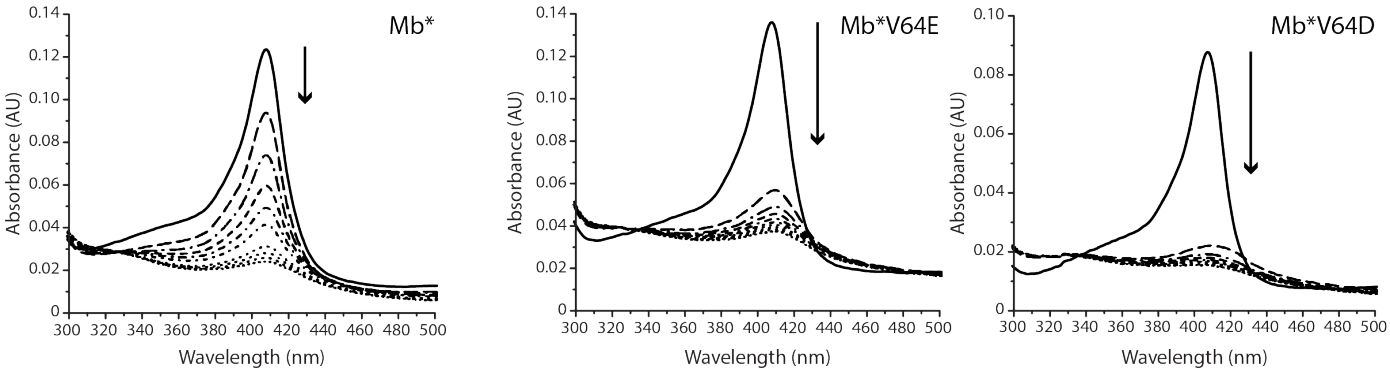

Figure 2-9 ***Time series UV/VIS spectra*** *of Mb** ***(left)****, Mb*V64E* ***(middle)****, and Mb*V64D* ***(right)*** *upon addition of either 3.5 mM (Mb*) or 140 µM (Mb*V64E, Mb*V64D) hydrogen peroxide. Each increasingly dashed line represents the passing of 1 minute.*

In the case of the Mb*[(Mn)ppIX] a marked difference between mCPBA and hydrogen peroxide oxidation was observed (*Figure 2-10*). Using mCPBA, the Soret peak at 370 nm was quickly replaced by a novel peak at 410 nm after 5 minutes. However, using either 140 µM, 0.5 mM, 3.5 mM, 10 mM or 100 mM of hydrogen peroxide, the spectrum remained unchanged. This difference in reactivity may explain the poor reactivity of the manganese protein variants that was observed when using hydrogen peroxide as the oxidant (Section 2.3.6).

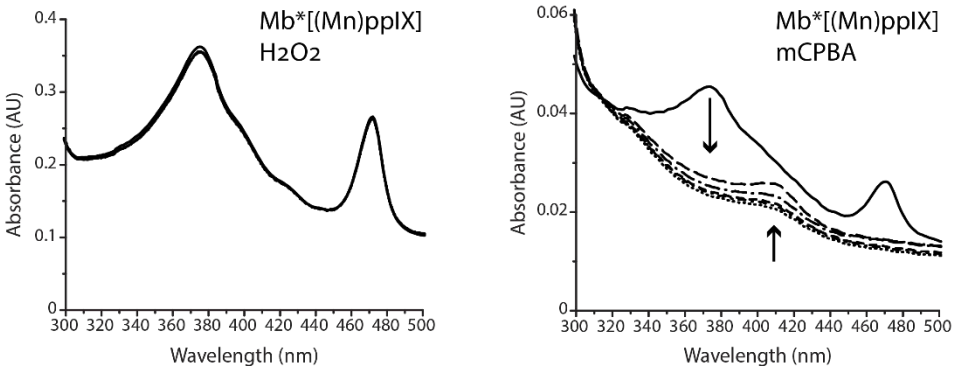

Figure 2-10 ***Time series UV/VIS spectra*** *of Mb*[(Mn)ppIX] upon addition of either 3.5 mM H_2O_2* ***(left)*** *or 14µM mCPBA* ***(right)****. Each increasingly dashed line represents the passing of 1 minute.*

2.3.5 Phenol Red Assay

Representative Mb* variants (Mb*, Mb*H93C, Mb*V64D, Mb*H93C V64D and Mb*A68D) were screened by the phenol red assay. In this colorimetric reaction, phenol red is brominated yielding the blue product bromophenol blue (*Figure 2-11*). None of the variants showed any ability to catalyze this reaction. It was not possible to use mCPBA instead of hydrogen peroxide as the oxidant, since under these altered conditions the reaction proceeded within seconds, precluding it from use in determining enzyme activities.

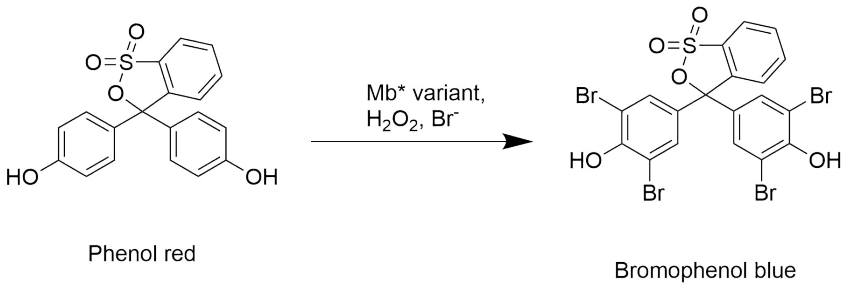

Figure 2-11 ***Reaction scheme showing the bromination of phenol red.***

2.3.6 Halogenation Activity in Monochlorodimedone (MCD) Assay

The expressed Mb* variants were screened for halogenation activity by using a modified monochlorodimedone (MCD) assay [34]. This assay is used as the benchmark for determining chloroperoxidase activity. During the reaction, MCD is chlorinated (*Figure 2-12*) and the decrease of the substrate absorbance is monitored by UV spectroscopy at 278 nm.

Normally, it is performed at pH 2.75 using hydrogen peroxide as the oxidant. Since the Mb* variants are not stable at this low pH (Section 2.3.3), the pH was increased to 5.5. This led to a shift in the absorbance maximum of MCD from 278 nm to 292 nm. Furthermore, initial trials looked more promising when using mCPBA as the oxidant instead of hydrogen peroxide. However, the reaction shows a background rate with mCPBA (4.6 nM/s) that is not present with H_2O_2. Nonetheless, activities over background could be observed.

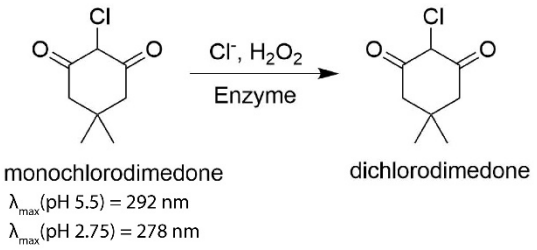

Figure 2-12 ***Reaction scheme for the MCD assay*** *together with the absorbance maxima of the substrate at pH 5.5 and pH 2.75.*

Several representative Mb* mutants were screened by the MCD assay using mCPBA as the oxidant. The results were evaluated by subtracting the background rate for each reaction and calculating the initial rate and total turnover number (*Figure 2-13*). All of the selected variants showed initial rates significantly above background. In most cases the total turnover number was proportional to the initial rate. Variants containing a catalytic base clearly outperform variants that do not, with the exception of Mb*V64E. The highest initial rate

(5.9 min^{-1}) and highest total turnover number (3.4) is achieved by Mb*V64D. The manganese containing Mb*[(Mn)ppIX] behaves similarly to its iron porphyrin containing counterpart. The chloroperoxidase performed poorly as compared to the data obtained with H_2O_2 when using mCPBA as the oxidant, even at its native pH of 2.75. At pH 5.5 no reaction above background could be observed.

In a subsequent experiment, various hydrogen peroxide concentrations were tested for compatibility with Mb*V64D (*Figure 2-14*). Activity was observed with 0.5 mM and 1 mM hydrogen peroxide. At the standard peroxide concentration of 2 mM, Mb*V64D showed no activity. Based on these results, new assay conditions were conservatively set to 0.5 mM hydrogen peroxide. This avoided the background reactivity of mCPBA and increased the comparability to the chloroperoxidase operating under its optimal conditions.

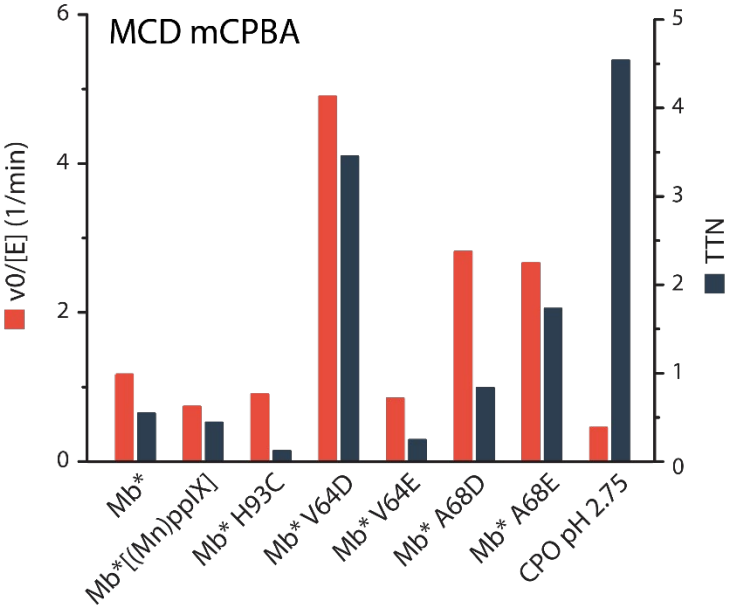

Figure 2-13 *Initial rates **(red)** and total turnover numbers **(blue)** of select Mb* variant in the **MCD assay using 14 µM mCPBA**, 20 µM MCD, 20 mM KCl and 1 µM enzyme at pH 5.5 (except CPO).*

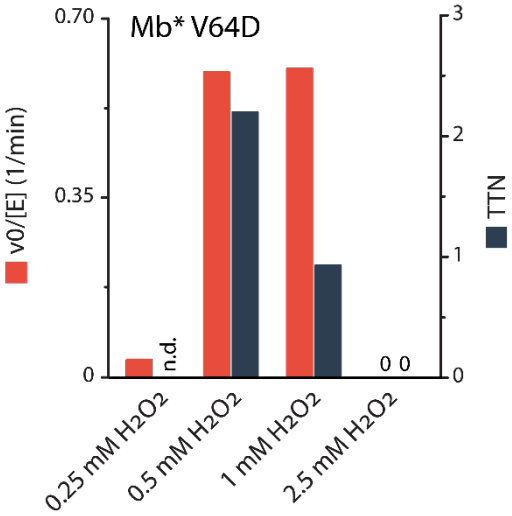

Figure 2-14 *Initial rates **(red)** and total turnover numbers **(blue)** of Mb*V64D in the **MCD assay** using 20 µM MCD, 20 mM KCl, 1 µM enzyme and **H_2O_2 concentrations ranging from 0.25 mM to 2.5 mM** at pH 5.5.*

A second, more comprehensive screening of the Mb* variants was conducted using hydrogen peroxide as the oxidant. As before, the results were evaluated in terms of initial rate and total turnover number (*Figure 2-15*). Most initial rates were 2-5 times lower when using hydrogen peroxide instead of mCPBA. Despite this, the total turnover numbers remained comparable. Mb*V64D, the variant with the highest initial rate with mCPBA, remains faster than most of the other variants. Surprisingly, all variants are vastly outperformed in terms of initial rate by Mb*A68D (17 min^{-1}), which even bests the chloroperoxidase in its native conditions of pH 2.75. However, it fails to achieve more than 8 turnovers per active site. In contrast, the chloroperoxidase boasts a total turnover number above 90. At pH 5.5 it behaves comparably to the average Mb* variant. Due to the quickly diminishing initial rate, it was difficult to determine rates for Mb*A68D accurately using the UV/VIS spectrometer. Since around 10 seconds elapsed after the addition of enzyme before measurement and the values were determined conservatively, the rates for Mb*A69D should be seen as lower bounds. The manganese porphyrin variants again fail to improve on their iron porphyrin counterparts.

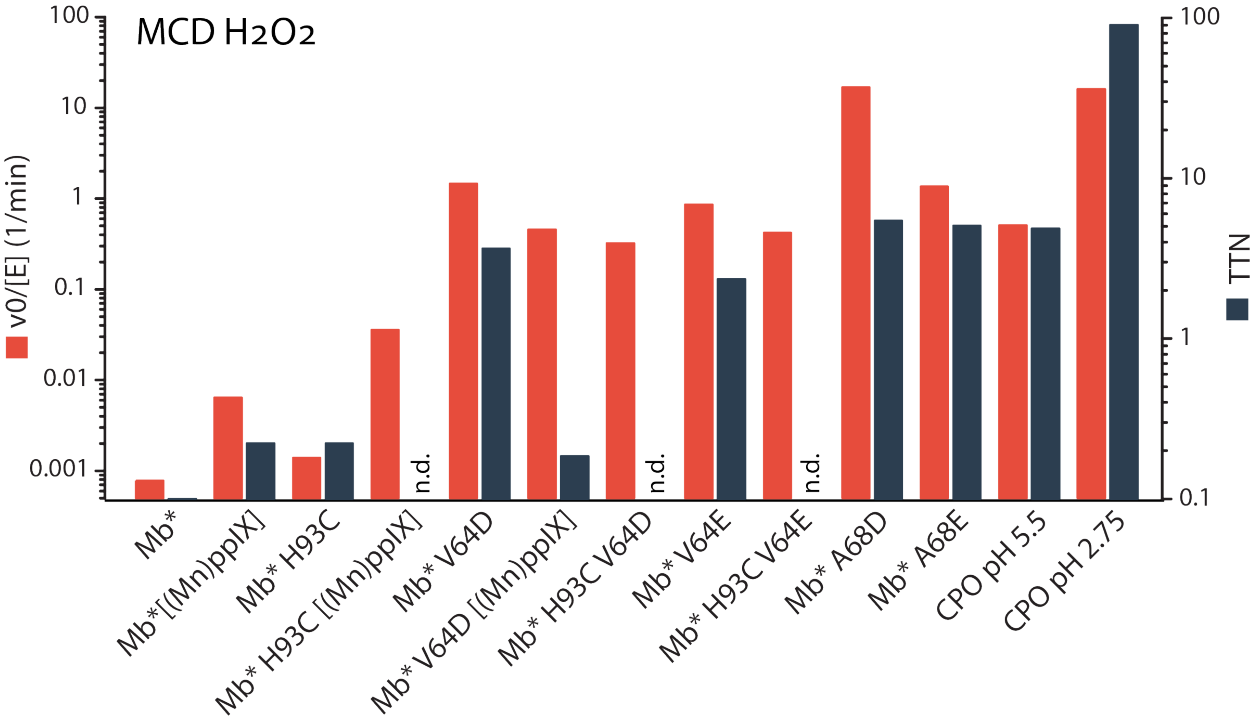

Figure 2-15 *Compilation of initial rates **(red)** and total turnover numbers **(blue)** of Mb* variants in the **MCD assay** using 20 µM MCD, 20 mM KCl, 0.5 mM H_2O_2 and 1 µM enzyme at pH 5.5 (except CPO).*

Based on the high initial rate of A68D, an attempt was made to increase the total turnover number of the enzyme by optimizing the hydrogen peroxide concentration (*Figure 2-16*). A clear decrease in initial rate was observed with decreasing hydrogen peroxide concentration, with the rate at 50 µM peroxide being less than half of that at 500 µM. Conversely, the total turnover number increased at lower peroxide concentrations, reaching 12 at 100 µM of the oxidant. Further lowering of the peroxide concentration showed no additional improvement.

Finally, the MCD assay was also performed using bromide as the halogen source. The observed initial rates were 2-3-fold higher than when using chloride (*Figure 2-17*). The total turnover numbers remained comparable (data not shown). However, they seemed consistently proportional to the results obtained with chloride. Hence, no further systematic study was performed.

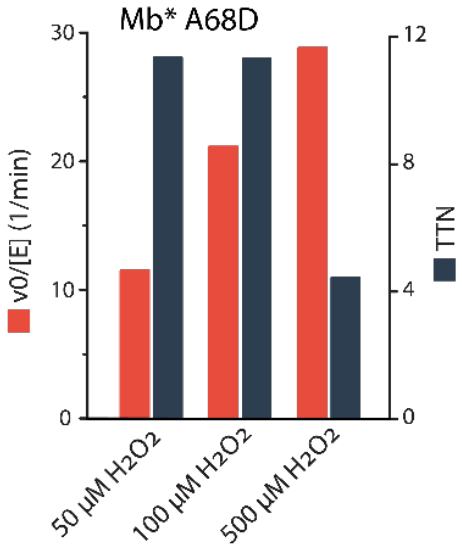

Figure 2-16 *Initial rates **(red)** and total turnover numbers **(blue)** of Mb*A68D in the **MCD assay** using 20 µM MCD, 20 mM KCl, 1 µM enzyme and **H_2O_2 concentrations ranging from 50 µM to 500 µM** at pH 5.5.*

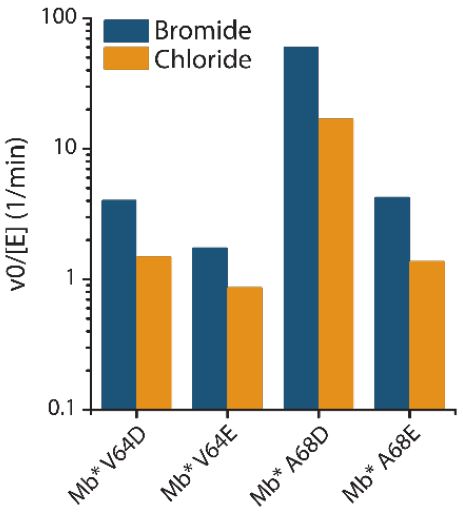

Figure 2-17 *Initial rate in the **MCD assay** of four Mb*V64D, Mb*V64E, Mb*A68D and Mb*A68E using 20 µM MCD, 0.5 mM H_2O_2, 0.5 µM enzyme and either 20 mM KBr **(blue)** or 20 mM KCl **(orange)** at pH 5.5*

2.3.7 pH Optima of Halogenase Activity

The pH optima for the MCD assay were determined for Mb*V64D/E and Mb*A68D/E by performing the assays in buffers of pH ranging from 3 to 7.4. The data were evaluated both in terms of initial rate and total turnover number (*Figure 2-18*). Both Mb*A68D and Mb*A68E displayed optima at pH 5.5 in terms of rate and turnover numbers, while Mb*V64E had its optimum at pH 5. In the case of Mb*V64D, maximal turnover was achieved at pH 5, while its rate seemed to be highest at pH 6. This experiment was conducted twice (newer version shown) but in both cases Mb*V64D didn't show the curved profile displayed by the other variants.

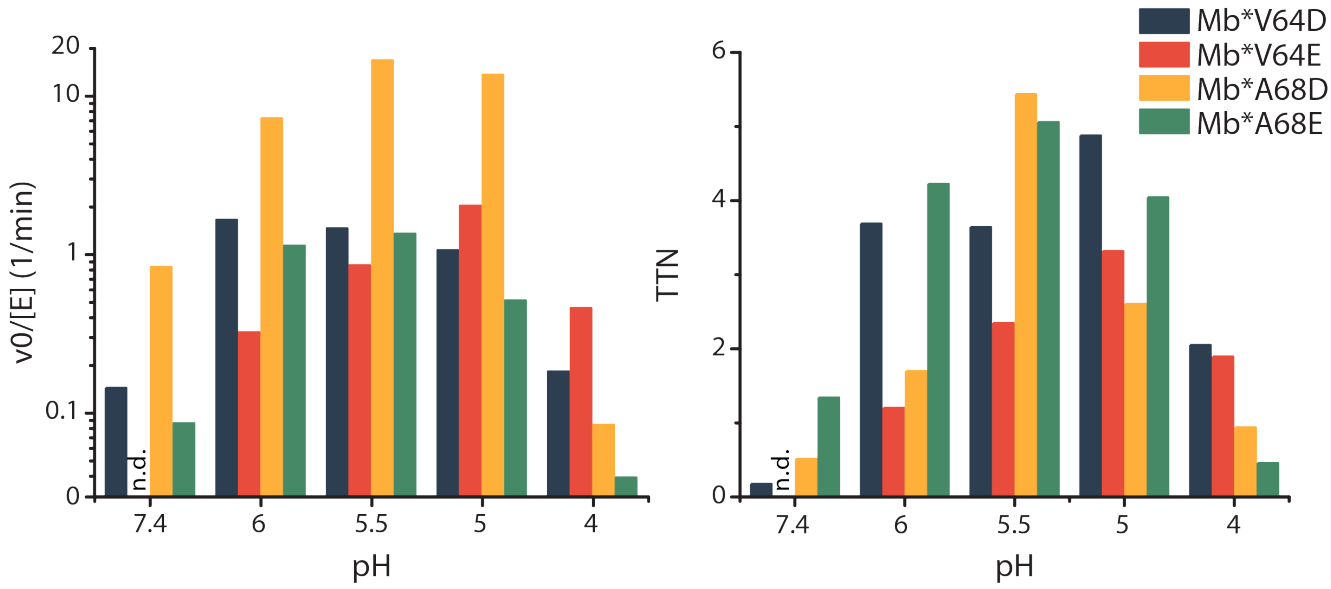

Figure 2-18 *Initial rates* ***(left)*** *and total turnover numbers* ***(right)*** *of four Mb* variants in the* ***MCD assay*** *using 20 µM MCD, 20 mM KCl, 0.5 mM H_2O_2 and 1 µM enzyme at* ***pH values ranging from 4 to 7.4****.*

2.3.8 Peroxidase Activity

To answer the question whether chlorination activity in the MCD assay is correlated with peroxidase activity, four separate peroxidase activity assays were evaluated for compatibility with Mb*V64D. In the guaiacol assay, *o*-methoxyphenol (guaiacol) is oxidized by the enzyme yielding a tetrameric product that absorbs at 470 nm [56]. The vanillic acid assay is based on the oxidation of 4-aminopyrine by hydrogen peroxide, followed by subsequent addition to vanillic acid yielding a quinoneimine dye which absorbs at 490 nm [60]. In the 2,2'-azino-bis(3-ethylbenzthiazoline-6-sulfonic acid) (ABTS) assay, the substrate is oxidized by the enzyme to a radical cation that absorbs strongly at 405 nm [61]. Finally, the N,N,N',N'-tetramethyl-p-phenylenediamine (TPMD) assay follows the formation of oxidized substrate at 563 nm [62].

The handling of the ABTS assay proved difficult due to the low solubility of the substrate. Furthermore, the product absorbance maximum overlapped with that of the enzyme Soret band, necessitating equilibration of the enzyme with hydrogen peroxide prior to the addition of substrate. The TMPD assay showed high levels of autoreactivity that were comparable to the rates detected. Based on these considerations, only the guaiacol and the vanillic acid assays were selected for further screening.

All expressed Mb* variants were screened by both guaiacol and vanillic acid assays to assess their peroxidase activities. The data were evaluated by calculating initial rates and total turnover numbers (*Figure 2-19*). There is a strong linear correlation between the initial rates measured in vanillic acid and MCD assays (*Figure 2-20*). Mb*A68D shows the highest initial rate of 129 min^{-1}, followed by Mb*V68D. The total turnover numbers observed with vanillic acid are two orders of magnitude higher as compared to MCD, with Mb*A68D reaching

over 1200 turnovers per active site. Interestingly, the chloroperoxidase shows almost no activity in the vanillic acid assay. Neither the cysteine nor the manganese containing variants display notable reactivity.

Surprisingly, the guaiacol assay shows a different trend (*Figure 2-19*, right). Here, both variants containing glutamate, Mb*V64E and Mb*A68E, outperform their aspartate containing counterparts in terms of both rate (5.8 min^{-1}) and turnovers (51). Except for these outliers, the situation is analogous to that observed in the vanillic acid and MCD assays. The chloroperoxidase shows a similar initial rate to Mb*A68D, albeit with half of the total turnovers. Again, both cysteine and manganese porphyrin containing variants lack reactivity altogether.

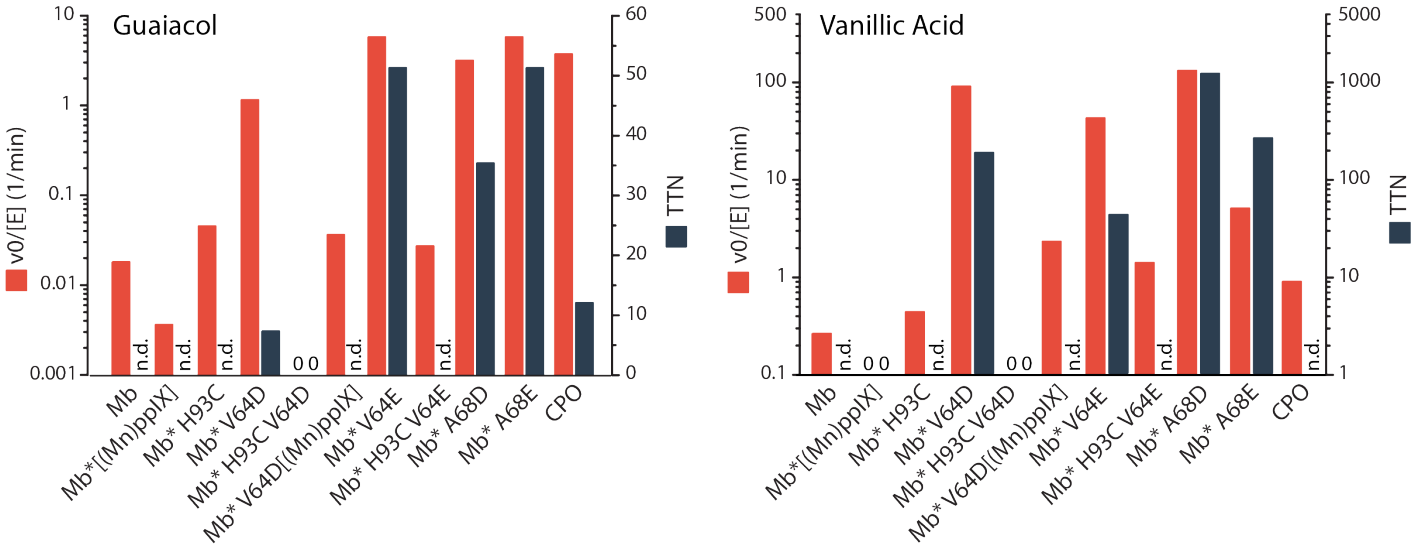

Figure 2-19 *Initial rates **(red)** and total turnover numbers **(blue)** of Mb* variants in **guaiacol** (**left**, 20 mM guaiacol, 0.5 mM H2O2, 1 µM enzyme, pH 7.4) and **vanillic acid** (**right**, 1 mM of vanillic acid, 0.75 mM 4-aminoantipyrine, 0.5 mM H_2O_2, 1 µM enzyme, pH 7.4) assays.*

Further investigation showed that the hydrogen peroxide concentration of 0.5 mM was rate limiting in the guaiacol assay for the fastest variant Mb*V64E. Various H_2O_2 concentrations were tested to optimize the enzymes performance *(Figure 2-21)*. The initial rate of the enzyme increased with higher peroxide concentrations up to a concentration of 10 mM which are 7-fold faster than those at 0.5 mM. At 20 mM hydrogen peroxide the rate declined again, suggesting that the enzyme is unstable at this concentration. The total turnover numbers, which are highest at low H_2O_2 concentrations and continuously decrease above 5 mM peroxide, support this interpretation.

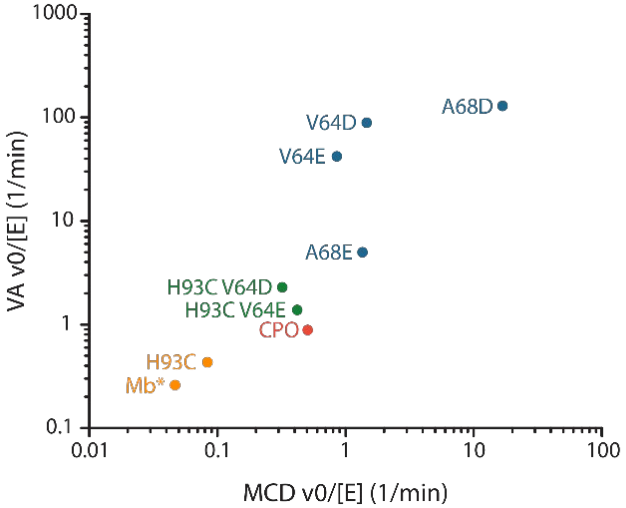

Figure 2-20 ***Correlation plot of Mb* variants** comparing initial rate in the MCD assay **(x-axis)** with initial rate in vanillic acid assay **(y-axis).** The values for CPO were measured at pH 5.5 in the MCD assay and pH 7.4 in the vanillic acid assay.*

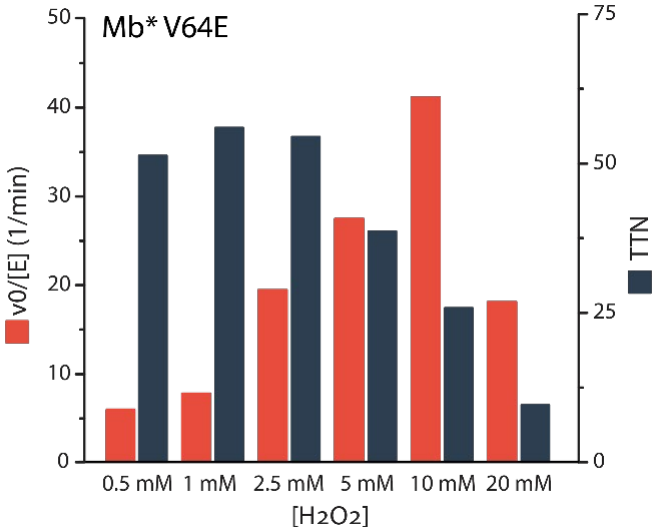

Figure 2-21 *Initial rates **(red)** and total turnover numbers **(blue)** of Mb*V64E in the **guaiacol assay** using 20 mM guaiacol, 0.5 µM enzyme and **H_2O_2 concentrations ranging from 0.5 mM to 20 mM** at pH 7.4.*

3. Discussion

3.1. Protein Expression and Porphyrin Loading

The systematic mutagenesis study performed on the myoglobin active site by Hargrove *et al.* [50] is a valuable resource for analyzing the porphyrin loading of the Mb* variants generated here. In their report, replacement of F43 with either tryptophan, valine, leucine or isoleucine led to an increase in porphyrin dissociation of over 10-fold as compared to the wild type. In hemoglobin, loss of the conserved phenylalanine is associated with several pathologies resulting from increased porphyrin dissociation and the presence of additional water molecules in the active site pocket. The decreased heme affinity additionally causes greater protein unfolding in the F43V mutant. In this work, the installation of the polar aspartate or glutamate in the Mb*F43D/E variants could promote excess water in the active site, possibly lowering protein stability. Subsequent aggregation of proteins and formation of inclusion bodies may explain the low yields obtained upon purification (*Table 2-1*).

In the Hargrove study, position H64 seemed to be sensitive to replacement by either small apolar amino acids (G,A,L) as well as large aromatics (W,Y) with these substitutions increasing porphyrin dissociation over 10-fold as compared to the wild type. However, installation of valine, isoleucine, phenylalanine or glutamine at H64 was well tolerated. The stable nature of Mb*V64D/E seems to agree with these trends described by Hargrove *et al*. It is perhaps nonetheless surprising that a negative charge can be introduced at this position where the wild type contains a histidine.

According to Hargrove *et al.*, position V68 was almost completely insensitive to replacement by both small apolar (A,L,I), aromatic (F,W) as well as polar (S,T) and charged (N,Q) residues as measured by porphyrin dissociation. This insensitivity, especially to large aromatic residues, seems to indicate that there is a fair amount of space available around position 68, or at least that the protein can create such space if necessary. It is tempting to speculate if this is related to the superior halogenation ability of Mb*A68D. Perhaps this freedom in positioning allows the residue to adopt a more optimal configuration as compared to Mb*V64D.

Hargrove *et al.* reported that replacement of H93 by glycine increased porphyrin dissociation by nearly 1000-fold. This matches the very low porphyrin loading of H93G measured here (*Table 2-1*). The mutant can be rescued by the addition of imidazole or other suitable ligands to the buffer [51]. It is then able to serve as a model system for investigating the effects of various proximal ligands on enzyme activity [63]. As Liu *et al.* [64] credit the nature of the proximal ligand as a decisive factor for the reactivity of their manganese porphyrin catalyst, investigation along these lines may prove worthwhile.

3.2. pH Stability of Mb* Variants

The heme dissociated from Mb* at pH 4.5, from Mb*V64D at pH 4 and from Mb*H93C V64D at pH 3 (*Figure 2-7, Figure 2-8*). The fact that Mb*V64D seems to be more pH stable than Mb* matches the Hargrove data, where replacement of H64 by valine (as in Mb*) is less favorable than replacement by the charged glutamine. It is unclear why Mb*H93C V64D should be more stable than either of the other two variants, especially given the apparent low porphyrin loading of H93C mutants and the higher pKa of cysteine as compared to histidine.

3.3. Rate of Compound I Formation

The rate of compound I formation was observed to be fastest in Mb*V64D, followed by Mb*V64E and much slower in Mb* (*Figure 2-9*). These relative rates track the relative reactivities of these variants observed in both the MCD and vanillic acid assays. This is consistent with the proposed catalytic cycles for both reactions which proceed through compound I. Additional support for the required hydrogen peroxide deprotonation step is given by the extremely slow rate of compound I formation in Mb*, which lacks a potential catalytic base.

A discrepancy in compound I formation was observed in Mb*[(Mn)ppIX] between using mCPBA and hydrogen peroxide (*Figure 2-10*). While addition of mCPBA caused a rapid change in the UV/VIS spectrum, hydrogen peroxide had no effect on the spectral properties of the enzyme. The lack of the formation of a reactive species in manganese reconstituted myoglobin variants accords with the findings of Cai *et al.* [45] who report no observable epoxidation activity with H_2O_2. The mechanism for this reaction also proceeds through compound I. Further, they could rescue the activity by use of the alternative oxidant oxone. However, in an earlier publication [46], the same researchers demonstrated spectral changes in manganese reconstituted wild type myoglobin upon addition of 20 equivalents of H_2O_2. They noted that the conversion to compound I was much slower than in iron porphyrin containing enzymes. It is therefore possible that the combination of the manganese porphyrin together with the use of a variant containing no potential catalytic base simply makes the reaction too slow to observe under the conditions used in this study.

In any case, there seems to be a marked difference in the reactivity towards H_2O_2 between manganese and iron porphyrin variants. This likely explains the low activities of the manganese variants in both halogenation and peroxidase assays when using H_2O_2 as the oxidant. The data from the compound I formation experiment as well as the findings of Cai *et al.* [45] suggest that the investigation of alternative water compatible oxidants may be worthwhile.

3.4. Bromination Activity

It is surprising that all measured Mb* variants can perform bromination at higher rates than chlorination in the MCD assay (*Figure 2-17*), yet none of them shows positive results on the phenol red assay (Section 2.3.5). Aside from the different substrate, the assay conditions only differ in the use of acetate buffer rather than phosphate and the use of higher halide concentrations. Since phenol red reacts with hypobromite, this seems to suggest that no hypobromite is produced by the Mb* variants. The activity of these variants with bromide in the MCD assay would then have to be explained by another mechanism.

An intriguing possibility is that the L-$Fe^{(III)}$-OBr species may react directly with the substrate. Under this hypothesis, MCD is small enough to enter the active site, while phenol red is not. Perhaps such reactivity is facilitated by a higher pKa of the potential catalytic base in in the Mb* variants (see 3.7), hindering protonation of the L-$Fe^{(III)}$-OBr, as compared to the perturbed glutamate in the chloroperoxidase. This hypothesis could be tested by more extensive substrate screening under a variety of pH values. If this were indeed the case, one could expect to be able to achieve stereo- and regioselectivities in the Mb* system not seen in the chloroperoxidase which predominantly uses free hypohalite as the halogenating species.

3.5. Halogenation Activity

The Mb*A68D variant has an initial rate (17 min^{-1}) that is 1-2 orders of magnitude above that of all other variants (*Figure 2-15*). However, its total turnover number (8) is comparable to that of similar variants. It's initial rate (at pH 5.5) even matches that of the purchased chloroperoxidase at its pH optimum of pH 2.75. Nevertheless, the chloroperoxidase performs over 10 times as many turnovers. Under conditions optimized for maximal turnovers per active site, Mb*A68D peaked at 12 (*Figure 2-16*). Clearly, it would be desirable to engineer Mb*A68D towards higher total turnover numbers so that it can exploit its high initial rate.

It was difficult to determine the initial rate of Mb*A68D accurately using the UV/VIS spectrometer due to its magnitude combined with the quick inactivation of the enzyme. Since over 10 seconds elapsed between enzyme addition and measurement, the obtained values should be regarded as lower bounds. Over the course of the performed experiments the determined rates ranged from 17-30 min^{-1} under equivalent conditions. While no single value should be taken too seriously, the actual rate likely lies within or above this range. Future investigation will need to use a stopped-flow instrument instead of a UV/VIS spectrometer for determining rates accurately.

There is a large discrepancy between the measured initial rate of the purchased chloroperoxidase (*Figure 2-15*) and the values reported in the literature, both measured at pH 2.75. Hager *et al.* report a v0/[E] value of over 200 s^{-1} [34] (calculated from their data) which is almost 3 orders of magnitude above the value measured here. This difference likely stems from a combination of factors. First, Hager *et al.* used 2 mM H_2O_2 instead of the 0.5 mM H_2O_2 used here. It is likely that the lower peroxide concentrations are rate-limiting for the chloroperoxidase. Second, Hager et al. used 100 µM substrate and 2.4 nM enzyme, while the experiment in this thesis used 20 µM substrate and 175 nM enzyme. It is possible that at this reduced enzyme to substrate ratio, the enzyme is not yet fully saturated. Finally, Hager *et al.* used a crystalline enzyme preparation which likely exceeded the purchased CPO in purity.

Despite the much lower values measured for the chloroperoxidase under the assay conditions used, it is beneficial to have a direct comparison to the Mb* variants which are limited in their tolerance of higher H_2O_2 concentrations. The fact that the chloroperoxidase is capable of much higher rates with increased H_2O_2 concentrations seems to suggest that Mb*A68D too could show higher rates if it could be made more peroxide tolerant. Auto-inactivation further diminishes the total turnover numbers achieved by Mb*A68D. Such auto-inactivation might proceed through the halogenation of active site residues leading to inactivation of catalytic residues or the expulsion of the porphyrin due to disruption of favorable interactions. Furthermore, the porphyrin itself may be halogenated leading to a loss in catalytic activity or expulsion. These issues may be mitigated by increasing the substrate to enzyme ratio.

3.6. Comparison of pH Optima for Halogenation Activity

The pH optima in the MCD assay were determined to be at pH 5.5 for Mb*A68D and Mb*A68E, while Mb*V64E showed an optimum at pH 5 (*Figure 2-18*). The pKa values for the side chains of apartate and glutamate in solution are 3.7 and 4.2 respectively [65]. The proposed mechanism for halogenation by the chloroperoxidase requires the catalytic residue to act both as a base to deprotonate H_2O_2 during its coordination to the iron center, as well as an acid during hypohalous acid release. If this mechanism is correct, one would expect the pH optimum of the enzyme to correspond with the pKa of the catalytic residue barring other factors. This bears out well in the case of the chloroperoxidase.

For the Mb* variants this does not seem true. Both Mb*A68D and Mb*A68E show the same optimum despite the different pKas of their potential catalytic residues. Furthermore, the optimum of Mb*V64E is lower than that of Mb*V64D, despite the higher value expected based on the higher pKa of the free glutamate compared to aspartate. It is important to note that these optima are likely independent of enzyme stability, since measured rates and turnovers already decline at pH values above those determined to be critical for stability (Section 2.3.3).

The generally higher pH optima in the Mb* variants compared to the chloroperoxidase can be explained by the lack of histidine that coordinates the catalytic residue in the former. In the chloroperoxidase, this interaction leads to a lowering of glutamate pKa. Nonetheless, this leaves the inconsistency of the relative optima of the Mb* variants unexplained. Perhaps positioning effects and local environment play a larger role than the identity of the amino acid.

3.7. Peroxidase Activity

The peroxidase activities (*Figure 2-19*) generally correspond with the trends observed in the MCD assay. Specifically, the vanillic acid assay shows a strong linear correlation to the MCD data (*Figure 2-20*) with Mb*A68D (129 min^{-1}, 1200) outperforming all other variants. In contrast to the MCD assay, Mb*A68D is capable of up to 10 times as many turnovers as other comparable variants. There seems to be much less of a problem with enzyme inactivation in this assay as compared to the MCD assay. Surprisingly, the chloroperoxidase seems to be unable to catalyze this reaction.

In the guaiacol assay (*Figure 2-19*, left) both Mb*V64E (5.8 min^{-1}, 51) and Mb*A68E (5.8 min^{-1}, 51) show higher rates and turnover numbers than Mb*A68D (3.2 min^{-1}, 40). This is an outlier compared to the other assays. Perhaps these glutamate bearing variants are more efficiently reduced to compound II. As is the case with the vanillic acid assay, inactivation of the enzyme seems to be less problematic than in the MCD assay.

The chloroperoxidase performs comparably to Mb*A68D in term of initial rate (3.7 min^{-1}). In contrast to the halogenation assay, it only achieves half the turnovers of Mb*A68D. While the relative activities between Mb*A68D and CPO are consistent between assays, there is again a large discrepancy between the measured values and those found in the literature. Thomas *et al.* [39] report an initial rate of 37.5 s^{-1} for CPO in the guaiacol assay which is 500-fold higher than that measured here. Similar factors as those discussed above (Section 3.5) are likely at work here. Specifically, the H_2O_2 concentration is likely to be of importance since even Mb*V64E was shown to be rate-limited by the peroxide concentration.

Pott *et al.* [56] reported an initial rate of 60 min^{-1} and total turnover number of 140 for wild type myoglobin using 10 mM H_2O_2 in the guaiacol assay. This is comparable to the 7-fold increased rate (41 min^{-1}) achieved for Mb*V64E under optimized peroxide concentrations of 10 mM (*Figure 2-21*). The Mb* variant, however, only achieves 26 turnovers at this H_2O_2 concentration. This means that the best Mb* variant is still a worse peroxidase than the wild type enzyme. It is likely that the stability that has been sacrificed through mutation to Mb*V64E cannot be compensated by any benefits those mutations provide.

4. Conclusion and Outlook

The planned Mb* variants were generated and screened for both halogenation (MCD assay) and peroxidase activities (guaiacol and vanillic acid assays). Mb*A68D vastly outperformed all other variants with an initial rate of up to 30 min^{-1} during the MCD assay matching even that of the chloroperoxidase, albeit with 10-fold lower total turnovers of up to 12. Variants bearing cysteine as proximal ligand showed low porphyrin loading and activities that were barely measurable. The manganese-porphyrin reconstituted variants all showed lower activity than their iron containing counterparts potentially due to their coordination to unsuitable proximal ligands.

The dependence of enzyme activity on proximal ligand could be investigated using the cavity mutant Mb*H93G. In this model system, exogenous ligands can be coordinated to the porphyrin [63]. For example, it may be possible to generate manganese porphyrin intermediates with either hydroxide or fluoride as proximal ligand. These could potentially perform chlorinations and fluorinations analogous to those described by Liu *et al.* [40], [43] (Section 1.4). Situating such reactions within an enzyme active site would mimic the apolar milieu of organic solvents while simultaneously providing increased regio- and stereocontrol.

Having established the lead variant Mb*A68D, a broader investigation of its activity is in order. Specifically, the enzyme should be tested for compatibility with substrates known to be halogenated by the chloroperoxidase. These include other diketones, aromatic amino acids, substituted phenols, anilines, alkenes and alkynes. Tryptophan, in particular, would enable comparison of the generated heme-dependent halogenase with naturally occurring flavin-dependent halogenases. The regioselectivity of halogenation in the Mb* variant could thus be contrasted with that of thoroughly investigated enzymes such as PrnA.

The performance of Mb*A68D is hampered by its instability under higher H_2O_2 concentrations along with its fast rate of inactivation during the halogenation assay. A thorough investigation of what mechanisms are at work during inactivation may aid in overcoming the low total turnover numbers observed. Specifically, it would be important to determine which sites, if any, on the enzyme or porphyrin are predominantly halogenated. Should the problem prove intractable by rational methods, the use of random mutagenesis combined with screening for total turnover may yield results.

The differences in activity between the use of H_2O_2 and mCPBA suggest that alternative mechanism may operate depending on the choice of oxidant. Investigation along these lines may help determinine the nature of the halogenating species. If conditions can be found where halogenation takes place using an enzyme-bound intermediate, this would provide a unique opportunity for engineering stereo- and regioselectivities that would be impossible in the chloroperoxidase. For example, a specific substrate binding site could be incorporated into the enzyme.

Finally, peroxidase activity corresponded well with observed halogenase activity, with a strong linear correlation being observed between vanillic acid and MCD assays. This suggests that good peroxidases also perform well as halogenases through efficient formation of the common intermediate compound I. The establishment of a link between the two activities creates the possibility of screening natural peroxidases for halogenase activity. Moreover, the lessons learned in improving peroxidase activity may also be applicable to halogenases in general. The extensive literature on both myoglobin and peroxidases thus provides a wealth of knowledge that can be put to combined use in developing efficient myoglobin-derived halogenases.

5. Materials and Methods

5.1. Molecular Biology

5.1.1 Medium Preparation

LB and 2xYT media were prepared from culture broth powder according to manufacturer instructions followed by autoclaving. Unless otherwise specified kanamycin was used at 25 µg/mL. Pre-prepared kanamycin positive culture plates were obtained from the general lab stock.

5.1.2 Buffer Preparation

5.1.2.1 PBS

PBS was prepared by making a 10x stock solution (1.37 M NaCl, 27 mM KCl, 100 mM Na2HPO4, 20 mM KH2PO4) which was adjusted to pH 7.4.

5.1.2.2 Nickel-NTA Buffers

Nickel-NTA wash buffer was prepared (50 mM Tris, 300 mM NaCl, 10 mM Imidazole) and adjusted to pH 8. Nickel-NTA elution buffer was prepared (50 mM Tris, 300 mM NaCl, 300 mM Imidazole) and adjusted to pH 8.

5.1.2.3 TSS Buffer

TSS buffer (12.5 mM PEG 8000, 30 mM MgCl2, 5% v/v DMSO in LB medium) was prepared and filter sterilized (0.22 µm)

5.1.3 Chloroperoxidase

C. fumago chloroperoxidase was purchased from Sigma. Its concentration was determined to be 23.5 mg/mL based on porphyrin absorbance at 403 nm (ε = 75300 $M^{-1}cm^{-1}$ [66], 40.5 kDa). Its loading was calculated to be 32% based on the ratio of the concentration determined by porphyrin absorbance and the concentration determined by absorbance at 280 nm (ε = 45450 $M^{-1}cm^{-1}$, aatbio.com tool).

5.1.4 Production of Chemically Competent *E. coli*

A 5 mL seed culture of either XL1-Blue or BL21 *E. coli* cells was grown to saturation in LB medium. 1 mL of this culture was diluted back into 50 mL of LB medium and grown to an optical density of 0.2-0.5. The culture was incubated on ice for 10 minutes and pelleted (10 min, 3000 *g*, 4°C). The supernatant was removed, and the cells were resuspended in 5 mL chilled, filter sterilized TSS buffer. The resulting cell suspension was aliquoted (100 µL) into chilled Eppendorf tubes and stored at -80°C.

5.1.5 Plasmid Vector and Mb H64V V68A (Mb*) Gene Sequence

A pET29b vector including a kanamycin resistance gene was used to express the myoglobin variants bearing an N-terminal $(His)_6$ tag under an IPTG inducible T7 promoter. The following DNA sequence was used to express the Mb* protein:

5'-ATGATGGTTCTGTCTGAAGGTGAATGGCAGCTGGTTCTGCATGTTTGGGCTAAAGTTGAAGCTGACGTCGCTGGTCATGGTCAG
GACATCTTGATTCGACTGTTCAAATCTCATCCGGAAACTCTGGAAAAATTCGATCGTTTCAAACATCTGAAAACTGAAGCTGAAATGA
AAGCTTCTGAAGATCTGAAAAAAGTGGGTGTTACCGCGTTAACTGCCCTAGGTGCTATCCTTAAGAAAAAAGGGCATCATGAAGCT
GAGCTCAAACCGCTTGCACAATCGCATGCTACTAAACATAAGATCCCGATCAAATACCTGGAATTCATCTCTGAAGCGATCATCCATG
TTCTGCATTCTAGACATCCAGGTGACTTCGGTGCTGACGCTCAGGGTGCTATGAACAAAGCTCTGGAGCTGTTCCGTAAAGATATCG
CTGCTAAGTACAAAGAACTGGGTTACCAGGGTGGCTCGGGACATCATCACCATCACCATTGAGTTTAACTCGAGCACCACCACCACC
ACCAC-3'

5.1.6 Quickchange PCR

Primers for PCR were designed using the Agilent quickchange online tool (*https://www.chem.agilent.com/store/primerDesignProgram.jsp*) and ordered from Microsynth.

Primer Name	Primer Sequence
Mb*H93C_fw	5'-GGG ATC TTA TGT TTA GTA GCA CAC GAT TGT GCA AGC GGT TTG AG-3'
Mb*H93C_rv	5'-CTC AAA CCG CTT GCA CAA TCG TGT GCT ACT AAA CAT AAG ATC CC-3'
Mb*V64D_fw	5'-AGT TAA CGC GGT AAC ACC ATC TTT TTT CAG ATC TTC AGA AGC TTT CA-3'
Mb*V64D_rv	5'-TGA AAG CTT CTG AAG ATC TGA AAA AAG ATG GTG TTA CCG CGT TAA CT-3'
Mb*V64E_fw	5'-AAC GCG GTA ACA CCC TCT TTT TTC AGA TCT TCA GAA G-3'
Mb*V64E_rv	5'-CTT CTG AAG ATC TGA AAA AAG AGG GTG TTA CCG CGT T-3'
Mb*F43D_fw	5'-CAG ATG TTT GAA ACG ATC GTC TTT TTC CAG AGT TTC CGG ATG AGA TTT-3'
Mb*F43D_rv	5'-AAA TCT CAT CCG GAA ACT CTG GAA AAA GAC GAT CGT TTC AAA CAT CTG-3'
Mb*F43E_fw	5'-AGT TTT CAG ATG TTT GAA ACG ATC CTC TTT TTC CAG AGT TTC CGG ATG AGA TTT G-3'
Mb*F43E_rv	5'-CAA ATC TCA TCC GGA AAC TCT GGA AAA AGA GGA TCG TTT CAA ACA TCT GAA AAC T-3'
Mb*V68D_fw	5'-ATA GCA CCT AGG GCA GTT AAA TCG GTA ACA CCC ACT TTT TTC-3'
Mb*V68D_rv	5'-GAA AAA AGT GGG TGT TAC CGA TTT AAC TGC CCT AGG TGC TAT-3'
Mb*A68E_fw	5'-CAC CTA GGG CAG TTA ACT CGG TAA CAC CCA CTT TT-3'
Mb*A68E_rv	5'-AAA AGT GGG TGT TAC CGA GTT AAC TGC CCT AGG TG-3'
Mb*H93G_fw	5'-GGA TCT TAT GTT TAG TAG CAC CCG ATT GTG CAA GCG GTT TGA-3'
Mb*H93G_rv	5'-TCA AAC CGC TTG CAC AAT CGG GTG CTA CTA AAC ATA AGA TCC-3'

Table 5-1 *List of the forward **(fw)** and reverse **(rv)** primer sequences used for quickchange PCR.*

Standard PCR reactions were preformed using 2.5 µL each of forward and reverse primers (10 µM), 10 µL 5x Phusion Buffer, 1 µL of 10 mM dNTPs, 0.5 µL Template DNA (at around 100 ng/µL), 1 µL Phusion High-Fidelity DNA polymerase and H_2O up to 50 µL. The reactions were run with an initial denaturation step at 98°C for 30 seconds, 16 cycles of denaturation at 98°C for 5 seconds, annealed at recommended annealing temperature for 20 seconds and elongated at 72°C for 20 s/kb. The final elongation was performed at 72°C for 8 minutes followed by holding at 4°C. The PCR products were treated for 2 hours with 1 µL DpnI after adding 5 µL of CutSmart buffer.

5.1.7 Transformation into XL1-Blue *E. coli*

An aliquot (50 µL) of chemically competent XL1-Blue cells were thawed on ice. Following addition of 5 µL PCR product, cells were incubated on ice for 5 minutes and heat-shocked at 42°C for 45 seconds. After recovery on ice for 2 minutes, 250 µL LB medium was added, followed by an hour of incubation at 37°C. The transformed cells were plated onto pre-warmed kanamycin plates and grown at 37°C overnight.

5.1.8 Miniprep and Sequencing

An individual colony was used to inoculate 5 mL LB + kanamycin and was grown overnight at 37°C. A glycerol stock was prepared from the single clone XL1-Blue culture by mixing 250 µL of culture with 250 µL sterile 50 % glycerol in a cryo tube to be stored at -80°C. The remaining cells were miniprepped (Zymo Research Miniprep Classic) according to manufacturer instructions. Part of the plasmid DNA was sent for sequencing using a primer complementary to the T7 promoter.

5.1.9 Transformation into BL21 *E. coli*

After confirmation by sequencing, the plasmid was transformed into BL21 cells according to the procedure described above (insert reference). Individual colonies were picked, and glycerol stocks were prepared.

5.2. Protein Production

5.2.1 Protein Expression

Precultures were inoculated from BL21 glycerol cell stock in 3 mL LB + kanamycin and grown overnight at 37°C. Using 1 mL preculture, either 100 mL or 1 L of 2xYT + kanamycin was inoculated and grown to an OD of 0.5 at 37°C. Expression was induced using 100 µM IPTG, 1 mM δ-aminolevulinic acid was added and cells were left to produce at 25°C for 24 hours. Cells were harvested by centrifugation at 10'000 *g* for 30 minutes.

5.2.2 Protein Purification by Nickel-NTA

The cell pellet was resuspended in 30 mL PBS, transferred to a falcon tube on ice and lysed by sonication (2x 1.5 min, 0.6 cycle, 80% power). In the case of 1 L expression cultures, the pellet was split into 3 separate 30 mL portions prior to sonication. To each falcon 330 µL of 20 mM hemin chloride in 10mM NaOH was added. The lysate was centrifuged (10 min, 7'000 *g*) and the supernatant was loaded onto Nickel-NTA resin (3 mL, Quiagen) equilibrated with wash buffer. The loaded resin was washed with two column volumes of wash buffer. The protein was eluted with 4-5 mL elution buffer. The eluted protein was dialyzed against PBS overnight using a 10 kDa molecular weight cutoff membrane.

5.2.3 Size Exclusion Chromatography

A Superdex 75 column (GE) (stored in 20% ethanol) was first equilibrated with 30 mL degassed ddH_2O followed by equilibration with 30 mL filtered and degassed PBS. In the case of 1 L expression cultures, 700 µL of the dialyzed protein was filtered using spin filters (0.22 µm) and injected into the FPLC. A pre-established protocol was run (Matthias Tinzl). The proteins generally eluted around 13-16 mL displaying a small pre-peak of aggregates. The fractions containing the main peak were collected and stored at 4°C.

5.2.4 Protein Storage

Proteins were stored in PBS at 4°C for up to one month. For longer term storage, proteins were aliquoted into 500 µL, flash frozen in liquid nitrogen and stored at -80°C.

5.2.5 SDS-PAGE

An appropriate volume of 5x reducing SDS loading buffer (200 mM Tris-HCl pH 6.8, 10% (w/v) SDS, 0.02% (w/v) bromophenol blue, 5% (v/v) β-mercaptoethanol, 20% (v/v) glycerol) was added to the protein sample followed by boiling at 95°C for 5 minutes. SDS-PAGE was run on 20 % PhastGel (GE) using a PhastSystem gel separation and development unit.

5.2.6 Calculation of Protein Concentrations

The concentrations of Mb* variants were calculated based on porphyrin absorbance. The absorbance was measured by Nanodrop at 410 nm (ε = 157000 $M^{-1}cm^{-1}$ [44]) for variants bearing histidine as proximal ligand and at 391 nm (ε = 100000 $M^{-1}cm^{-1}$ [57]) for variants bearing a cysteine as proximal ligand. Manganese porphyrin concentration was calculated based on the absorbance at 470 nm (ε = 60000 $M^{-1}cm^{-1}$ [44]). Porphyrin loading was determined by taking the ratio of the concentration determined by porphyrin absorbance and the concentration determined by absorbance at 280 nm (ε = 15220 $M^{-1}cm^{-1}$, aatbio.com tool).

5.2.7 Apo-Protein Production

Solutions of 10 mM NaH_2PO_4, 1 M HCl as well a 2-butanone were cooled on ice. In a 15 mL falcon tube, 0.5 mL of dialyzed protein and 1.5 mL of 10 mM NaH_2PO_4 were mixed, followed by addition of 60 µL of 1 M HCl. Immediately afterwards, 2 mL of 2-butanone were added. The falcon was shaken for 30 s and the phases were allowed to separate for 5 minutes. In cases were the phases did not separate neatly, the sample was centrifuged briefly. The upper 2-butanone phase was siphoned off and the extraction was repeated an additional time. After the second extraction, the aqueous phase was spin filtered (0.22 µm) and purified by size exclusion chromatography.

5.2.8 Manganese$^{(III)}$ Protoporphyrin reconstitution

To the purified apo-protein, 10 % (v/v) of a Mn$^{(III)}$-protophorphyrin IX solution (2 mg/mL in methanol) was added. The sample was incubated for 1-2 hours on ice, spin filtered (0.22 µm) and by purified by size exclusion chromatography.

5.3. Activity Assays

5.3.1 General UV Methods

UV/VIS spectroscopy was performed on a Perkin Elmer lambda series spectrometer. A background correction was taken using buffer. After each addition, the cuvette was inverted five times.

5.3.2 Phenol Red Assay

The phenol red assay was conducted by adding 1 mM H_2O_2 followed by 1 µM or 0.1 µM enzyme to a prepared assay solution (1 M NaAc pH 5.5, 1 M NaBr, 0.002 % phenol red) and by measuring absorbance increase at 562 nm in a 1 cm cuvette over time.

5.3.3 Monochlorodimedone (MCD) Assay

In a 0.5 cm cuvette either 20 mM KCl or 20 mM KBr was added to a 0.1 M potassium phosphate buffer of desired pH (standard condition pH 5.5). After performing a background correction, 20 µM MCD (2-chloro-5,5-dimethyl-1.3-cyclohexanedione, 100x in methanol) and 0.5 mM H_2O_2 was added. The cuvette was inverted five times and the absorbance was checked for stability. After addition of either 1 µM or 0.1 µM enzyme, the cuvette was inverted five times and the absorbance decrease at 292 nm was monitored. The extinction coefficient of MCD at 292 nm in aqueous buffer at pH 5.5 was determined to be 54000 $M^{-1}cm^{-1}$. In the case of measuring in buffer of pH 2.75, the absorbance was monitored at 278 nm (ε = 12200 $M^{-1}cm^{-1}$ [34]) due to the shift in the absorbance maximum of MCD. The identity of the dichlorinated product was verified by LC-MS.

5.3.4 Guaiacol Assay

In a 1 cm cuvette containing PBS, 20 mM guaiacol, H_2O_2 (1 mM or 0.5 mM) and enzyme (1 µM or 0.1 µM) were added in that order. The absorbance increase at 470 nm (ε = 22000 $M^{-1}cm^{-1}$ [56]) was monitored.

5.3.5 Vanillic Acid and 4-aminoantipyrine Assay

In a 1 cm cuvette containing 0.1 M potassium phosphate buffer at pH 7.4, 1 mM of vanillic acid was added followed by 0.75 mM of 4-aminoantipyrine, by H_2O_2 (1 mM or 0.5 mM) and finally by enzyme (1 µM or 0.1 µM). The absorbance increase was monitored at 490 nm (ε = 4656 $M^{-1}cm^{-1}$ [60]).

5.3.6 2,2'-azino-bis(3-ethylbenzthiazoline-6-sulfonic acid) (ABTS) Assay

In a 1 cm cuvette containing 0.1 M phosphate buffer at pH 5, either 1 µM or 0.1 µM of enzyme was added, followed by 1 mM H_2O_2. An absorbance decrease at 405 nm was observed due to depletion of the porphyrin Soret band. Once the absorbance stabilized, 9.1 mM of ABTS was added and the absorbance increase at 405 nm (ε = 36800 $M^{-1}cm^{-1}$ [61]) was monitored.

5.3.7 N,N,N',N'-tetramethyl-p-phenylenediamine (TMPD) Assay

In a 1 cm cuvette containing 0.1 M phosphate buffer at pH 6, 20 mM TMPD (dissolved in 0.1 M K_2PO_4 at pH 3 to slow autoreactivity) was added followed by 1 mM H_2O_2 and finally by either 1 µM or 0.1 µM enzyme. The absorbance increase at 563 nm (ε = 11700 $M^{-1}cm^{-1}$ [62]) was monitored.

5.4. Chemical Syntheses

5.4.1 General

Unless otherwise stated all reactions were carried out under nitrogen atmosphere.

5.4.2 Synthesis of Protoporphyrin IX

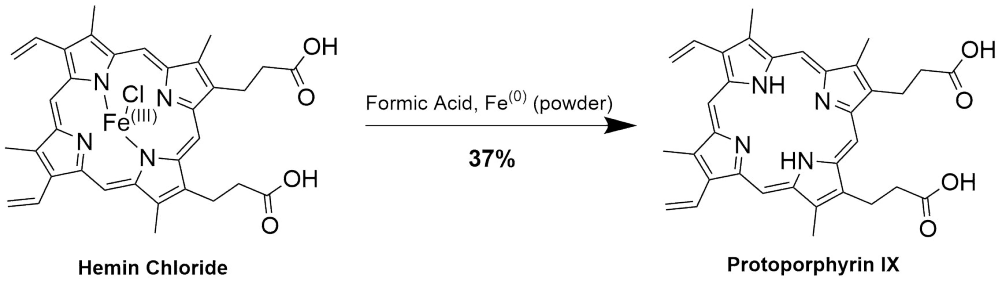

Hemin Chloride — Protoporphyrin IX

Scheme 5-1 ***Synthesis of protoporphyrin IX from hemin chloride.***

Protoporphyrin IX was synthesized according to a modified literature procedure [67]. To a refluxing solution of hemin chloride (3 g, 4.6 mmol, 1 eq.) in 150 mL formic acid, six portions of 0.5 g iron powder (total 3 g, 54 mmol, 11.7 eq.) were added in 5-minute intervals. After the last addition, the solution was cooked for an additional 15 minutes and then cooled to room temperature. The remaining iron was filtered off. Water (375 mL), along with around 75 g of solid ammonium acetate was added to the filtrate. After letting the filtrate settle, the precipitate was filtered off, washed thoroughly with water, collected and transferred to a 50 mL falcon tube. The precipitate was washed with ethanol, followed by centrifugation. After two wash steps, the pellet was dried under vacuum overnight. The dried pellet was dissolved in as little acetic acid as possible (80 mL). Roughly 150 mL of a 40 % (w/v) sodium hydroxide solution was added, until the pH exceeded 13 and precipitation occurred. The brown oily precipitate was filtered off, dried at 120°C, collected from the filter and dried under vacuum overnight.

The dried precipitate was dissolved in concentrated hydrochloric acid, and extracted several times with a 1:3 pyridine:chloroform mixture. Care was taken to make sure that the solution had neutralized completely before collecting the extracted organic phases. The product was concentrated under vacuum. To remove residual pyridine from the product, 150 mL of toluene was added and removed completely under vacuum three times. The product was identified by UV/VIS and mass spectroscopy (Appendix 8.1, ESI: $[M+H]^+$, calc: 563.2653, meas.: 563.2650). Product purity was estimated to be 80% based on the residual pyridine absorbance peak and comparison with the UV/VIS spectrum of commercial protoporphyrin IX ($\varepsilon_{400(MeOH)}$= 83300 $M^{-1}cm^{-1}$, calculated). From this estimate, the yield was calculated to be 37 %.

5.4.3 Synthesis of Manganese(III) Protoporphyrin IX

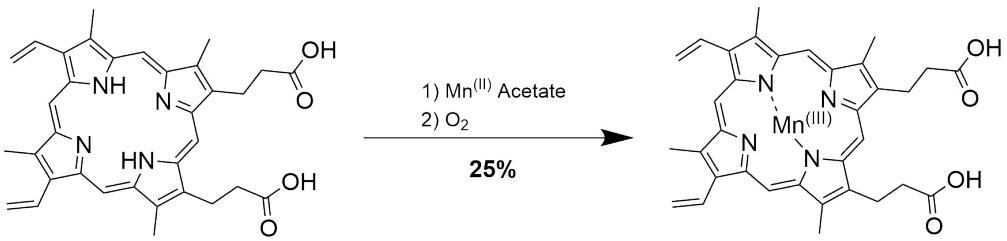

Protoporphyrin IX — Manganese (III) Protoporphyrin IX

Scheme 5-2 ***Synthesis of manganese protoporphyrin IX from protoporphyrin IX.***

Manganese protoporphyrin IX was synthesized according to a modified literature procedure [68]. A refluxing solution of manganous acetate (200 mg, 1.15 mmol, 6.4 eq.) in 60 % acetic acid (10 mL) was siphoned into a refluxing solution of protoporphyrin IX (100 mg, 0.18 mmol, 1 eq.) in glacial acetic acid (10 mL) through a piece

of teflon tubing. After 10 minutes of stirring, the combined solution was aerated for 5 minutes using a syringe. The reaction was quenched by first adding 120 mL of saturated NaCl followed by 70 mL of water. The brown solution was refrigerated overnight. The newly formed precipitate was collected by centrifugation, washed twice with 25 % NaCl and three times with water in a 50 mL falcon tube. After the final wash the supernatant was removed and the precipitated was dried under vacuum over NaOH. A pyridine-chloroform-water-isooctane (50:25:25:2.5, v/v) mixture was prepared. A celite column was prepared by suspending column material in the upper phase, packing the column and equilibrating with the lower phase. The dried precipitate was dissolved in the lower phase and run on the celite column. The blood red initial band was collected, dried under vacuum, re-dissolved in methanol, transferred to a 50 mL falcon tube and dried again. The resulting material was washed twice with 25 % NaCl, 4 times with 5 % HCl, once again with 25 % NaCl and 4 times with water. After the final wash step, the supernatant was removed and the product dried under vacuum over NaOH. The product was identified by UV/VIS and mass spectroscopy (Appendix 8.2, ESI: $[M]^+$, calc.: 615.1799, meas.: 615.1798). Product purity was estimated to be 60% based on comparison of the product UV/VIS spectrum with that of the starting material. From this estimate, the yield was calculated to be 25 % at 60 % conversion.

6. Acknowledgements

I would like to sincerely thank professors Hilvert and Kast for the opportunity of pursuing my Master Thesis in their lab. Furthermore, I would like to thank Matthias Tinzl for his competent supervision of this project. He provided a supportive atmosphere and was always available for advice. Finally, I would like to thank all Hilvert/Kast group members for their helpfulness in orienting me in the lab.

7. References

[1] A. de Meijere and F. Diederich, Eds., *Metal-Catalyzed Cross-Coupling Reactions*. Weinheim, Germany: Wiley-VCH Verlag GmbH, 2004.

[2] A. H. Cherney, N. T. Kadunce, and S. E. Reisman, "Enantioselective and Enantiospecific Transition-Metal-Catalyzed Cross-Coupling Reactions of Organometallic Reagents To Construct C–C Bonds," *Chem. Rev.*, vol. 115, no. 17, pp. 9587–9652, 2015.

[3] S. Purser, P. R. Moore, S. Swallow, and V. Gouverneur, "Fluorine in Medicinal Chemistry," *Chem. Soc. Rev.*, vol. 37, no. 2, pp. 320–330, 2008.

[4] G. Cavallo *et al.*, "The Halogen Bond," *Chem. Rev.*, vol. 116, no. 4, pp. 2478–2601, 2016.

[5] Y. Liu, W. Zhu, Y. Lu, K. Chen, Z. Xu, and Z. Yang, "Halogen Bond: Its Role beyond Drug–Target Binding Affinity for Drug Discovery and Development," *J. Chem. Inf. Model.*, vol. 54, no. 1, pp. 69–78, 2013.

[6] D. A. Petrone, J. Ye, and M. Lautens, "Modern Transition-Metal-Catalyzed Carbon-Halogen Bond Formation," *Chem. Rev.*, vol. 116, no. 14, pp. 8003–8104, 2016.

[7] D. K. Romney, F. H. Arnold, B. H. Lipshutz, and C. J. Li, "Chemistry Takes a Bath: Reactions in Aqueous Media," *J. Org. Chem.*, vol. 83, no. 14, pp. 7319–7322, 2018.

[8] M. T. Reetz, "Biocatalysis in Organic Chemistry and Biotechnology: Past, Present, and Future," *J. Am. Chem. Soc.*, vol. 135, no. 34, pp. 12480–12496, 2013.

[9] U. T. Bornscheuer, S. Lutz, K. Robins, R. J. Kazlauskas, G. W. Huisman, and J. C. Moore, "Engineering the Third Wave of Biocatalysis," *Nature*, vol. 485, no. 7397, pp. 185–194, 2012.

[10] C. K. Savile *et al.*, "Biocatalytic Asymmetric Synthesis of Sitagliptin Manufacture," *Science*, vol. 329, pp. 305–310, 2010.

[11] H. Renata, Z. J. Wang, and F. H. Arnold, "Expanding the Enzyme Universe: Accessing Non-Natural Reactions by Mechanism-Guided Directed Evolution," *Angew. Chemie - Int. Ed.*, vol. 54, no. 11, pp. 3351–3367, 2015.

[12] P. S. Huang, S. E. Boyken, and D. Baker, "The Coming of Age of de novo Protein Design," *Nature*, vol. 537, no. 7620, pp. 320–327, 2016.

[13] T. Mukai, M. J. Lajoie, M. Englert, and D. Söll, "Rewriting the Genetic Code," *Annu. Rev. Microbiol.*, vol. 71, no. 1, pp. 557–577, 2017.

[14] C. K. Prier and F. H. Arnold, "Chemomimetic Biocatalysis: Exploiting the Synthetic Potential of Cofactor-Dependent Enzymes to Create New Catalysts," *J. Am. Chem. Soc.*, vol. 137, no. 44, pp. 13992–14006, 2015.

[15] J. Latham, E. Brandenburger, S. A. Shepherd, B. R. K. Menon, and J. Micklefield, "Development of Halogenase Enzymes for Use in Synthesis," *Chem. Rev.*, vol. 118, no. 1, pp. 232–269, 2018.

[16] L. C. Blasiak and C. L. Drennan, "Structural Perspective on Enzymatic Halogenation," *Acc. Chem. Res.*, vol. 42, no. 1, pp. 147–155, 2009.

[17] V. Weichold, D. Milbredt, and K. H. van Pee, "Specific Enzymatic Halogenation - From the Discovery of Halogenated Enzymes to Their Applications In Vitro and In Vivo," *Angew. Chemie - Int. Ed.*, vol. 55, no. 22, pp. 6374–6389, 2016.

[18] G. W. Gribble, *Naturally Occurring Organohalogen Compounds - A Comprehensive Update*, vol. 91. Vienna: Springer Vienna, 2010.

[19] E. W. Schmidt, C. A. Bewley, and D. J. Faulkner, "Theopalauamide, a Bicyclic Glycopeptide from Filamentous Bacterial Symbionts of the Lithistid Sponge Theonella swinhoei from Palau and Mozambique," *J. Org. Chem.*, vol. 63, no. 4, pp. 1254–1258, 2002.

[20] L. Wang, X. Zhou, M. Fredimoses, S. Liao, and Y. Liu, "Naturally Occurring Organoiodines," *RSC Adv.*, vol. 4, no. 101, pp. 57350–57376, 2014.

[21] D. O'Hagan and D. B. Harper, "Fluorine-containing Natural Products," *J. Fluor. Chem.*, vol. 100, no. 1–2, pp. 127–133, 1999.

[22] V. Agarwal, Z. D. Miles, J. M. Winter, A. S. Eustáquio, A. A. El Gamal, and B. S. Moore, "Enzymatic Halogenation and Dehalogenation Reactions: Pervasive and Mechanistically Diverse," *Chem. Rev.*, vol. 117, no. 8, pp. 5619–5674, 2017.

[23] C. S. Neumann, D. G. Fujimori, and C. T. Walsh, "Halogenation Strategies In Natural Product Biosynthesis," *Chem. Biol.*, vol. 15, no. 2, pp. 99–109, 2008.

[24] D. O'Hagan and H. Deng, "Enzymatic Fluorination and Biotechnological Developments of the Fluorinase," *Chem. Rev.*, vol. 115, no. 2, pp. 634–649, 2015.

[25] P. D. Shaw and L. P. Hager, "An Enzymatic Chlorination Reaction," *J. Am. Chem. Soc.*, vol. 81, no. 4, pp. 1011–1012, 1959.

[26] C. Dong *et al.*, "Crystal Structure and Mechanism of a Bacterial Fluorinating Enzyme," *Nature*, vol. 427, no. 6974, pp. 561–565, 2004.

[27] M. Sundaramoorthy, "Chloroperoxidase," in *Handbook of Metalloproteins*, Chichester: John Wiley & Sons, Ltd, 2006.

[28] P. Kenigsberg, G.-H. Fang, and L. P. Hager, "Post-Translational Modifications of Chloroperoxidase from Caldariomyces fumago," *Arch. Biochem. Biophys.*, vol. 254, no. 2, pp. 409–415, May 1987.

[29] Q. Zong, P. A. Osmulski, and L. P. Hager, "High-Pressure-Assisted Reconstitution of Recombinant Chloroperoxidase," *Biochemistry*, vol. 34, no. 38, pp. 12420–12425, 1995.

[30] F. van Rantwijk, R. A. Sheldon, F. van de Velde, A. Conesa, P. J. Punt, and C. A. M. J. J. van den Hondel, " Expression of the Caldariomyces fumago Chloroperoxidase in Aspergillus niger and Characterization of the Recombinant Enzyme ," *J. Biol. Chem.*, vol. 276, no. 21, pp. 17635–17640, 2002.

[31] M. Sundaramoorthy, J. Terner, and T. L. Poulos, "The Crystal Structure of Chloroperoxidase: A Heme Peroxidase-Cytochrome P450 Functional Hybrid," *Structure*, vol. 3, no. 12, pp. 1367–1378, 1995.

[32] P. F. Hollenberg and L. P. Hager, "The P-450 Nature of the Carbon Monoxide Complex of Ferrous Chloroperoxidase," *J. Biol. Chem.*, vol. 248, no. 7, pp. 2630–2634, 1973.

[33] M. Sundaramoorthy, J. Terner, and T. L. Poulos, "Stereochemistry of the Chloroperoxidase Active Site: Crystallographic and Molecular-modeling Studies," *Chem. Biol.*, vol. 5, no. 9, pp. 461–473, 1998.

[34] L. P. Hager, D. R. Morris, F. S. Brown, and H. Eberwein, "Chloroperoxidase. II. Utilization of Halogen Anions," *J. Biol. Chem.*, vol. 241, no. 8, pp. 1769–1777, 1966.

[35] J. Geigert, S. L. Neidleman, D. J. Dalietos, and S. K. Dewitt, "Novel Haloperoxidase Reaction: Synthesis of Dihalogenated Products.," *Appl. Environ. Microbiol.*, vol. 45, no. 5, pp. 1575–81, May 1983.

[36] J. Geigert, S. L. Neidleman, and D. J. Dalietos, "Novel haloperoxidase substrates. Alkynes and cyclopropanes.," *J. Biol. Chem.*, vol. 258, no. 4, pp. 2273–7, Feb. 1983.

[37] M. D. Corbett, B. R. Chipko, and A. O. Batchelor, "The Action of Chloride Peroxidase on 4-Chloroaniline. N-oxidation and Ring Halogenation.," *Biochem. J.*, vol. 187, no. 3, pp. 893–903, Jun. 1980.

[38] F. S. Brown and L. P. Hager, "Chloroperoxidase. IV. Evidence for an Ionic Electrophilic Substitution Mechanism," *J. Am. Chem. Soc.*, vol. 89, no. 3, pp. 719–720, 1967.

[39] J. A. Thomas, D. R. Morris, and L. P. Hager, "Chloroperoxidase. VII. Classical Peroxidatic, Catalatic, and Halogenating Forms of the Enzyme.," *J. Biol. Chem.*, vol. 245, no. 12, pp. 3129–34, Jun. 1970.

[40] W. Liu and J. T. Groves, "Manganese Porphyrins Catalyze Selective C-H Bond Halogenations," *J. Am. Chem. Soc.*, vol. 132, no. 37, pp. 12847–12849, 2010.

[41] B. De Poorter, M. Ricci, O. Bortolini, and B. Meunier, "Catalytic Hydroxylation of Saturated Hydrocarbons with the Sodium Hypohalite/Manganese Porphyrin System," *J. Mol. Catal.*, vol. 31, no. 2, pp. 221–224, Jul. 1985.

[42] J. T. Groves, G. A. McClusky, R. E. White, and M. J. Coon, "Aliphatic Hydroxylation by Highly Purified Liver Microsomal Cytochrome P-450. Evidence for a Carbon Radical Intermediate," *Biochem. Biophys. Res. Commun.*, vol. 81, no. 1, pp. 154–160, 1978.

[43] W. Liu, X. Huang, M. J. Cheng, R. J. Nielsen, W. A. Goddard 3rd, and J. T. Groves, "Oxidative Aliphatic C-H Fluorination with Fluoride Ion Catalyzed by a Manganese Porphyrin," *Science*, vol. 337, pp. 1322–1325, 2012.

[44] G. Sreenilayam, E. J. Moore, V. Steck, and R. Fasan, "Metal Substitution Modulates the Reactivity and Extends the Reaction Scope of Myoglobin Carbene Transfer Catalysts," *Adv. Synth. Catal.*, vol. 359, no. 12, pp. 2076–2089, 2017.

[45] Y.-B. Cai, S.-Y. Yao, M. Hu, X. Liu, and J.-L. Zhang, "Manganese Protoporphyrin IX Reconstituted Myoglobin Capable of Epoxidation of the C=C Bond with Oxone," *Inorg. Chem. Front.*, vol. 3, no. 10, pp. 1236–1244, 2016.

[46] Y. B. Cai, X. H. Li, J. Jing, and J. L. Zhang, "Effect of Distal Histidines on Hydrogen Peroxide Activation by Manganese Reconstituted Myoglobin," *Metallomics*, vol. 5, no. 7, pp. 828–835, 2013.

[47] G. N. Phillips, "Myoglobin," in *Encyclopedia of Inorganic and Bioinorganic Chemistry*, vol. 39, no. 4, Chichester, UK: John Wiley & Sons, Ltd, 2011, pp. 527–532.

[48] B. A. Springer and S. G. Sligar, “High-Level Expression of Sperm Whale Myoglobin in Escherichia coli.,” *Proc. Natl. Acad. Sci.*, vol. 84, no. 24, pp. 8961–8965, Dec. 1987.

[49] J. C. Kendrew *et al.*, “Structure of Myoglobin: A Three-Dimensional Fourier Synthesis at 2 A Resolution.,” *Nature*, vol. 185, no. 4711, pp. 422–7, Feb. 1960.

[50] M. S. Hargrove, A. J. Wilkinson, and J. S. Olson, “Structural Factors Governing Hemin Dissociation from Metmyoglobin,” *Biochemistry*, vol. 35, no. 35, pp. 11300–11309, 1996.

[51] D. Barrick, “Replacement of the Proximal Ligand of Sperm Whale Myoglobin with Free Imidazole in the Mutant His-93→Gly,” *Biochemistry*, vol. 33, no. 21, pp. 6546–6554, 1994.

[52] S. B. J. Kan *et al.*, “Catalytic Iron-Carbene Intermediate Revealed in a Cytochrome c Carbene Transferase,” *Proc. Natl. Acad. Sci.*, vol. 115, no. 28, pp. 7308–7313, 2018.

[53] T. Hayashi *et al.*, “Capture and Characterization of a Reactive Haem–carbenoid Complex in an Artificial Metalloenzyme,” *Nat. Catal.*, vol. 1, no. 8, pp. 578–584, 2018.

[54] O. F. Brandenberg, R. Fasan, and F. H. Arnold, “Exploiting and Engineering Hemoproteins for Abiological Carbene and Nitrene Transfer Reactions,” *Curr. Opin. Biotechnol.*, vol. 47, pp. 102–111, 2017.

[55] J. G. Gober and E. M. Brustad, “Non-Natural Carbenoid and Nitrenoid Insertion Reactions Catalyzed by Heme Proteins,” *Curr. Opin. Chem. Biol.*, vol. 35, pp. 124–132, 2016.

[56] M. Pott, T. Hayashi, T. Mori, P. R. E. Mittl, A. P. Green, and D. Hilvert, “A Noncanonical Proximal Heme Ligand Affords an Efficient Peroxidase in a Globin Fold,” *J. Am. Chem. Soc.*, vol. 140, no. 4, pp. 1535–1543, 2018.

[57] T. Matsui, S. Nagano, K. Ishimori, Y. Watanabe, and I. Morishima, “Preparation and Reactions of Myoglobin Mutants Bearing Both Proximal Cysteine Ligand and Hydrophobic Distal Cavity: Protein Models for the Active Site of P-450,” *Biochemistry*, vol. 35, no. 40, pp. 13118–13124, 1996.

[58] T. Egawa, H. Shimada, and Y. Ishimura, “Formation of Compound I in the Reaction of Native Myoglobins with Hydrogen Peroxide,” *J. Biol. Chem.*, vol. 275, no. 45, pp. 34858–34866, 2000.

[59] H. P. Hersleth *et al.*, “Crystallographic and Spectroscopic Studies of Peroxide-Derived Myoglobin Compound II and Occurrence of Protonated FeIV-O,” *J. Biol. Chem.*, vol. 282, no. 32, pp. 23372–23386, 2007.

[60] A. Holt, D. F. Sharman, G. B. Baker, and M. M. Palcic, “A Continuous Spectrophotometric Assay for Monoamine Oxidase and Related Enzymes in Tissue Homogenates,” *Anal. Biochem.*, vol. 244, no. 2, pp. 384–392, 1997.

[61] Sigma, “Enzymatic Assay of PEROXIDASE (EC 1.11.1.7) 2,2’-Azino-bis(3-Ethylbenzthiazoline-6-Sulfonic Acid) as a Substrate.” 1996.

[62] W. Sun, T. A. Kadima, M. A. Pickard, and H. B. Dunford, “Catalase Activity of Chloroperoxidase and its Interaction with Peroxidase Activity,” *Biochem. Cell Biol.*, vol. 72, no. 7–8, pp. 321–331, 1994.

[63] J. Du, M. Sono, and J. H. Dawson, “The H93G Myoglobin Cavity Mutant as a Versatile Scaffold for Modeling Heme Iron Coordination Structures in Protein Active Sites and Their Characterization with Magnetic Circular Dichroism Spectroscopy,” *Coord. Chem. Rev.*, vol. 255, no. 7–8, pp. 700–716, 2011.

[64] W. Liu and J. T. Groves, “Manganese Catalyzed C-H Halogenation,” *Acc. Chem. Res.*, vol. 48, no. 6, pp. 1727–1735, 2015.

[65] “Wikipedia.” [Online]. Available: https://en.wikipedia.org/wiki/Amino_acid.

[66] D. R. Morris and L. P. Hager, “Chloroperoxidase. I. Isolation and Properties of the Crystalline Glycoprotein,” *J. Biol. Chem.*, vol. 241, no. 8, pp. 1763–1768, 1966.

[67] G. Schäfer, W. Schmidtmann, and K. H. Weiner, “Über die Identifizierung von enzymatisch gebildetem Hämin aus Protoporphyrin und Eisen,” *Hoppe-Seyler´s Zeitschrift für Physiol. Chemie*, vol. 328, no. Jahresband, pp. 269–271, 1962.

[68] T. A. Takashi Yonetani, “Studies on Cytochrome c Peroxidase,” *J. Biol. Chem.*, vol. 244, no. 17, pp. 4580–4588, 1969.

8. Appendix

8.1. MS Data: Synthesized Protoporphyrin IX

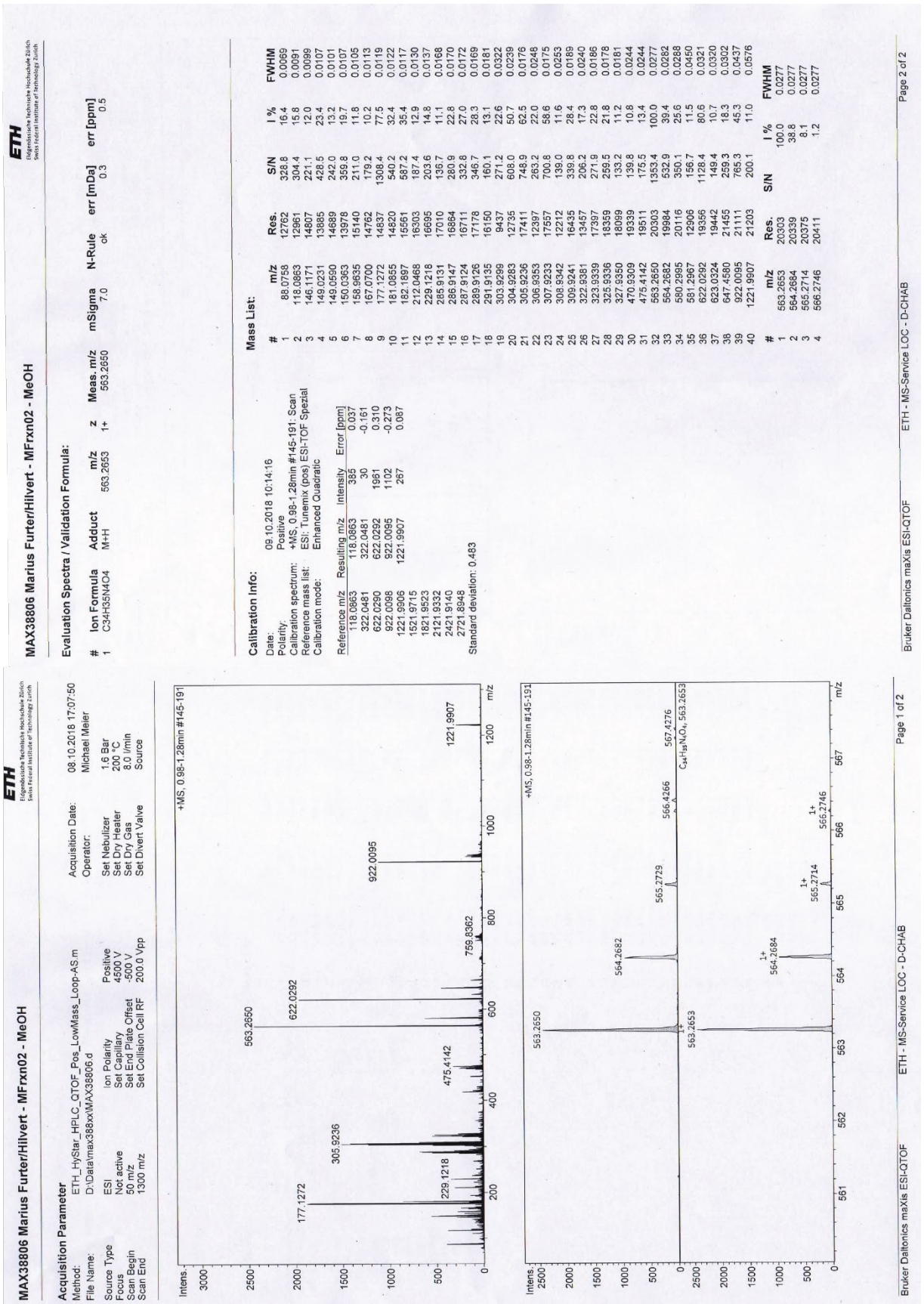

MAX38806 Marius Furter/Hilvert - MFrxn02 - MeOH

Acquisition Parameter

Method:	ETH_HyStar_HPLC_QTOF_Pos_LowMass_Loop-AS.m	Acquisition Date:	08.10.2018 17:07:50
File Name:	D:\Data\max388xx\MAX38806.d	Operator:	Michael Meier
Source Type	ESI	Ion Polarity	Positive
Focus	Not active	Set Capillary	4500 V
Scan Begin	50 m/z	Set End Plate Offset	-500 V
Scan End	1300 m/z	Set Collision Cell RF	200.0 Vpp
		Set Nebulizer	1.6 Bar
		Set Dry Heater	200 °C
		Set Dry Gas	8.0 l/min
		Set Divert Valve	Source

+MS, 0.98-1.28min #145-191

Intens.

m/z

Bruker Daltonics maXis ESI-QTOF | ETH - MS-Service LOC - D-CHAB | Page 1 of 2

MAX38806 Marius Furter/Hilvert - MFrxn02 - MeOH

Evaluation Spectra / Validation Formula:

#	Ion Formula	Adduct	m/z	z	Meas. m/z	mSigma	N-Rule	err [mDa]	err [ppm]
1	C34H35N4O4	M+H	563.2653	1+	563.2650	7.0	ok	0.3	0.5

Calibration Info:

Date:	09.10.2018 10:14:16
Polarity:	Positive
Calibration spectrum:	+MS, 0.98-1.28min #145-191: Scan
Reference mass list:	ESI: Tunemix (pos) ESI-TOF Spezial
Calibration mode:	Enhanced Quadratic

Reference m/z	Resulting m/z	Intensity	Error [ppm]
118.0863	118.0863	385	0.037
322.0481	322.0481	30	-0.161
622.0290	622.0292	1961	0.310
922.0098	922.0095	1102	-0.273
1221.9906	1221.9907	267	0.087
1521.9715			
1821.9523			
2121.9332			
2421.9140			
2721.8948			

Standard deviation: 0.483

Mass List:

#	m/z	Res.	S/N	I %	FWHM
1	88.0758	12762	328.8	16.4	0.0069
2	118.0863	12961	304.4	15.8	0.0091
3	146.1171	14807	221.1	12.0	0.0099
4	149.0231	13885	428.5	23.4	0.0107
5	149.0590	14689	242.0	13.2	0.0101
6	150.0363	13978	359.8	19.7	0.0107
7	158.9635	15140	211.0	11.8	0.0105
8	167.0700	14762	179.2	10.2	0.0113
9	177.1272	14837	1308.4	77.5	0.0119
10	181.0855	14820	540.2	32.4	0.0122
11	182.1897	15561	587.2	35.4	0.0117
12	212.0468	16303	187.4	12.9	0.0130
13	229.1218	16695	203.6	14.8	0.0137
14	285.9131	17010	136.7	11.1	0.0168
15	286.9147	16864	280.9	22.8	0.0170
16	287.9124	16711	332.8	27.0	0.0172
17	289.9126	17178	346.7	28.3	0.0169
18	291.9135	16150	160.1	13.1	0.0181
19	303.9299	9437	271.2	22.6	0.0322
20	304.9283	12735	608.0	50.7	0.0239
21	305.9236	17411	748.9	62.5	0.0176
22	306.9353	12397	263.2	22.0	0.0248
23	307.9233	17557	700.8	58.6	0.0175
24	308.9342	12212	139.0	11.6	0.0253
25	309.9241	16435	339.8	28.4	0.0189
26	322.9381	13457	206.2	17.3	0.0240
27	323.9339	17397	271.9	22.8	0.0186
28	325.9336	18359	259.5	21.8	0.0178
29	327.9350	18099	133.2	11.2	0.0181
30	470.9309	19339	139.8	10.8	0.0244
31	475.4142	19511	175.5	13.4	0.0244
32	563.2650	20303	1353.4	100.0	0.0277
33	564.2682	19984	532.9	39.4	0.0282
34	580.2995	20116	350.1	25.6	0.0288
35	581.2967	12906	156.7	11.5	0.0450
36	622.0292	19356	1128.4	80.6	0.0321
37	623.0324	19442	149.4	10.7	0.0320
38	647.4580	21455	259.3	18.3	0.0302
39	922.0095	21111	765.3	45.3	0.0437
40	1221.9907	21203	200.1	11.0	0.0576

#	m/z	Res.	S/N	I %	FWHM
1	563.2653	20303		100.0	0.0277
2	564.2684	20339		38.8	0.0277
3	565.2714	20375		8.1	0.0277
4	566.2746	20411		1.2	0.0277

Bruker Daltonics maXis ESI-QTOF | ETH - MS-Service LOC - D-CHAB | Page 2 of 2

BMAX001008 Marius Furter/Hilvert - MFrxn09 - MeOH - --

ETH Eidgenössische Technische Hochschule Zürich Swiss Federal Institute of Technology Zurich

Acquisition Parameter

Method:	ETH_HyStar_HPLC_QTOF_POS_LowMass_Loop-AS.m			Acquisition Date:	24.01.2019 14:42:12
File Name:	D:\Data\bmax0010xx\BMAX001008.d			Operator:	Michael Meier
Source Type	ESI	Ion Polarity	Positive	Set Nebulizer	1.6 Bar
Focus	Not active	Set Capillary	4500 V	Set Dry Heater	200 °C
Scan Begin	50 m/z	Set End Plate Offset	-500 V	Set Dry Gas	8.0 l/min
Scan End	1300 m/z	Set Collision Cell RF	200.0 Vpp	Set Divert Valve	Source

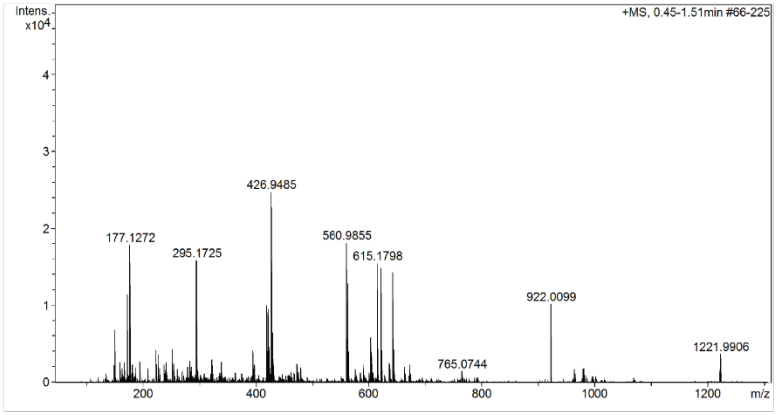

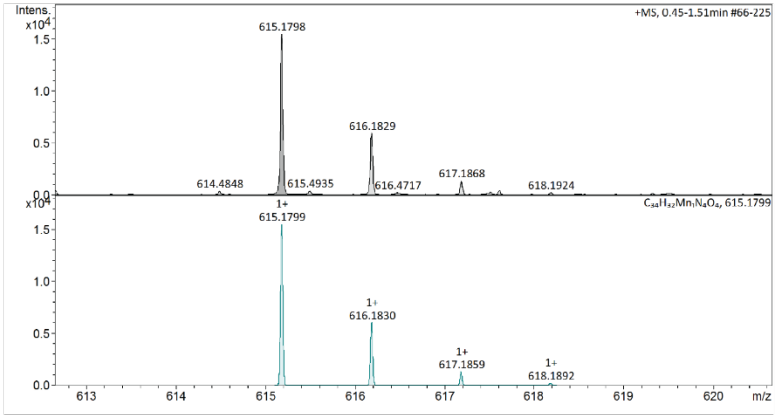

BMAX001008 Marius Furter/Hilvert - MFrxn09 - MeOH - --

ETH Eidgenössische Technische Hochschule Zürich Swiss Federal Institute of Technology Zurich

Evaluation Spectra / Validation Formula:

#	Ion Formula	Adduct	m/z	z	Meas. m/z	mSigma	N-Rule	err [mDa]	err [ppm]
1	C34H32MnN4O4	M	615.1799	1+	615.1798	4.2	-	-0.0	-0.0

Calibration Info:

Date:	24.01.2019 14:44:45
Polarity:	Positive
Calibration spectrum:	+MS, 0.45-1.51min #66-225: Scan
Reference mass list:	<Method>: Tunemix (pos) ESI-TOF Spezial
Calibration mode:	Enhanced Quadratic

Reference m/z	Resulting m/z	Intensity	Error [ppm]
118.0863	118.0863	149	-0.008
322.0481	322.0481	3012	0.042
622.0290	622.0289	14866	-0.086
922.0098	922.0099	10189	0.078
1221.9906	1221.9906	3711	-0.025
1521.9715			
1821.9523			
2121.9332			
2421.9140			
2721.8948			

Standard deviation: 0.134

Mass List:

#	m/z	Res.	S/N	I %	FWHM
1	150.0369	15643	5711.5	27.9	0.0096
2	158.9641	16020	1806.4	10.6	0.0099
3	167.9281	16707	1606.5	10.7	0.0101
4	172.8834	16139	6478.9	46.3	0.0107
5	177.1272	16137	9930.1	72.3	0.0110
6	194.1175	17374	1311.2	10.9	0.0112
7	223.2056	17863	1666.6	17.2	0.0125
8	227.1276	17404	1415.4	14.7	0.0131
9	240.9673	18206	944.8	10.4	0.0132
10	251.2369	18322	1530.2	17.5	0.0137
11	254.9829	17525	867.8	10.1	0.0146
12	283.0553	18227	815.8	11.2	0.0155
13	295.1725	18532	4396.1	64.1	0.0159
14	296.1758	18367	871.3	12.7	0.0161
15	322.0481	19205	654.2	12.2	0.0168
16	339.2318	19241	524.8	10.8	0.0176
17	394.9755	18365	614.9	16.8	0.0215
18	419.9539	20169	1290.5	40.5	0.0208
19	421.9537	19868	1215.7	38.8	0.0212
20	422.9567	18457	322.0	10.3	0.0229
21	423.9504	19499	576.9	18.4	0.0217
22	426.9485	20180	3099.3	100.0	0.0212
23	427.9516	19501	706.3	22.9	0.0219
24	428.9464	19951	1947.8	63.5	0.0215
25	429.9492	19739	419.6	13.8	0.0218
26	560.9855	20428	1613.7	73.4	0.0275
27	561.9882	20623	338.7	15.4	0.0272
28	562.9822	19821	303.3	13.8	0.0284
29	563.2653	21293	1148.4	52.2	0.0265
30	564.2684	21012	440.4	20.1	0.0269
31	603.9635	20745	528.0	23.9	0.0291
32	605.9600	20740	352.0	15.9	0.0292
33	615.1798	21366	1390.5	62.5	0.0288
34	616.1829	21312	530.8	23.8	0.0289
35	622.0289	20707	1348.2	60.2	0.0300
36	637.1619	21725	237.2	10.3	0.0293
37	643.2109	21670	1340.6	57.9	0.0297
38	644.2141	21606	539.8	23.3	0.0298
39	922.0099	21681	1802.3	41.2	0.0425
40	1221.9906	20674	1000.7	15.0	0.0591

#	m/z	Res.	S/N	I %	FWHM
1	615.1799	21366		100.0	0.0288
2	616.1830	21401		38.8	0.0288
3	617.1859	21436		8.1	0.0288
4	618.1892	21471		1.2	0.0288

8.3. Declaration of Independence

ETH

Eidgenössische Technische Hochschule Zürich
Swiss Federal Institute of Technology Zurich

Eigenständigkeitserklärung

Die unterzeichnete Eigenständigkeitserklärung ist Bestandteil jeder während des Studiums verfassten Semester-, Bachelor- und Master-Arbeit oder anderen Abschlussarbeit (auch der jeweils elektronischen Version).

Die Dozentinnen und Dozenten können auch für andere bei ihnen verfasste schriftliche Arbeiten eine Eigenständigkeitserklärung verlangen.

Ich bestätige, die vorliegende Arbeit selbständig und in eigenen Worten verfasst zu haben. Davon ausgenommen sind sprachliche und inhaltliche Korrekturvorschläge durch die Betreuer und Betreuerinnen der Arbeit.

Titel der Arbeit (in Druckschrift):

Engineering Myoglobin Towards Halogenase Activity

Verfasst von (in Druckschrift):

Bei Gruppenarbeiten sind die Namen aller Verfasserinnen und Verfasser erforderlich.

Name(n):	**Vorname(n):**
Fürter	Marius

Ich bestätige mit meiner Unterschrift:

- Ich habe keine im Merkblatt „Zitier-Knigge" beschriebene Form des Plagiats begangen.
- Ich habe alle Methoden, Daten und Arbeitsabläufe wahrheitsgetreu dokumentiert.
- Ich habe keine Daten manipuliert.
- Ich habe alle Personen erwähnt, welche die Arbeit wesentlich unterstützt haben.

Ich nehme zur Kenntnis, dass die Arbeit mit elektronischen Hilfsmitteln auf Plagiate überprüft werden kann.

Ort, Datum	**Unterschrift(en)**
Zürich, 24.3.19	

Bei Gruppenarbeiten sind die Namen aller Verfasserinnen und Verfasser erforderlich. Durch die Unterschriften bürgen sie gemeinsam für den gesamten Inhalt dieser schriftlichen Arbeit.